6

THE SURFACE CHEMICAL BOND

6.1 INTRODUCTION

We define the formation of a surface chemical bond to be adsorption accompanied by charge transfer and charge redistribution between the adsorbate and the substrate, producing strong bonds of covalent or ionic character. Heats of adsorption on the order of 63 kJ/mole (15 kcal/mole) or larger would certainly indicate the formation of a chemical bond, leading to long surface residence times τ [$\tau = \tau_0 \exp(\Delta H_{ads}/RT)$], even at elevated temperatures, compared to τ_0 ($\tau_0 \approx 10^{-12}$ sec) related to vibrational times for surface atoms.

Both surface atoms and adsorbates must participate to form the surface chemical bond. In order to determine the nature of the bond, the heat of adsorption is measured as a function of the pertinent variables. These include trends across the periodic table, variations of bond energies with adsorbate size, molecular structure and coverage, and substrate structure. Changes in the electronic and atomic structure of the bonding partners are determined and compared with their electronic and atomic (or molecular) structure before they formed the surface bond.

When a molecule from the gas phase adsorbs on a surface by forming a chemical

bond, the process is similar to a stoichiometric reaction. The product—the adsorbate—may resemble the gas-phase reactant; it may have greatly rearranged its bonding and, thus, its molecular structure; or it may have even dissociated on the surface. The other reactant—the surface—may have undergone similar changes: Its structure may be altered only slightly in the presence of the adsorbed molecule, or the surface atoms may have moved to new equilibrium positions by displacement perpendicular or parallel to the surface. Thus the surface may completely restructure as the adsorbate bonds form.

Some experimental techniques [e.g., low-energy electron diffraction (LEED)–surface crystallography] can detect the structural changes that occur on both sides of the surface chemical bond. However, most currently used techniques are only capable of detecting the structural changes that occur on the adsorbate side (e.g., infrared spectroscopy) or on the substrate side (e.g., electron microscopy). As a result, we often gain only incomplete information about the surface chemical bond, leading to a one-sided "molecule-centric" or "surface-centric" view of the adsorbate–surface compound that is produced.

The rest of this chapter reviews what is known about the nature of the surface chemical bond. It will become clear that a combination of techniques, which yield diverse information on the atomic, molecular, and electronic structure of the adsorbate–substrate compound, are needed to obtain a complete physical–chemical picture of bonding at surfaces and interfaces. We will summarize the information available and present the current models of the surface chemical bond, along with the unique properties of these bonds that have been uncovered by surface-science studies.

6.2 BONDING TRENDS ACROSS THE PERIODIC TABLE

Most available data of the heats of adsorption concern atoms (e.g., hydrogen, nitrogen, oxygen, and potassium) and small molecules (e.g., N_2, O_2, CO, and CO_2) on transition-metal surfaces. Some of the data are displayed in Figures 3.21–3.23. The heat of adsorption generally increases from right to left in the periodic table. This trend has been explained by the chemisorption model developed by Nørskov [1] using the effective-medium theory, whereby the interaction of the adsorbate with the metal is primarily determined by the so-called one-electron energy term. This term is defined as due to changes in the charge distribution of the atom or molecule when it is taken from a homogeneous electron gas (uniform charge) onto the surface. The main difference in a transition-metal surface is due to the *d*-electrons that lie in a band around the Fermi level. These *d*-states can interact with the adsorbate states, and thus hybridization can occur, giving rise to bonding and antibonding shifts. The *d*-electron contribution to the bonding is proportional to $(1 - f_d)$, where f_d is the degree of filling of the *d*-band. The *d*-electron contribution to the surface chemical bond depends on the degree of filling of the antibonding states (since the bonding states are already filled). Thus, early transition metals with fewer *d*-electrons form stronger chemical bonds. This effect is shown in Figure 6.1 for hydrogen and oxygen adsorbed on the 3*d* transition metals. The effective-medium theory provides good agreement between experimental data and calculated energies. Similar trends and agreement are found for the heats of adsorption of CO and N_2 as well.

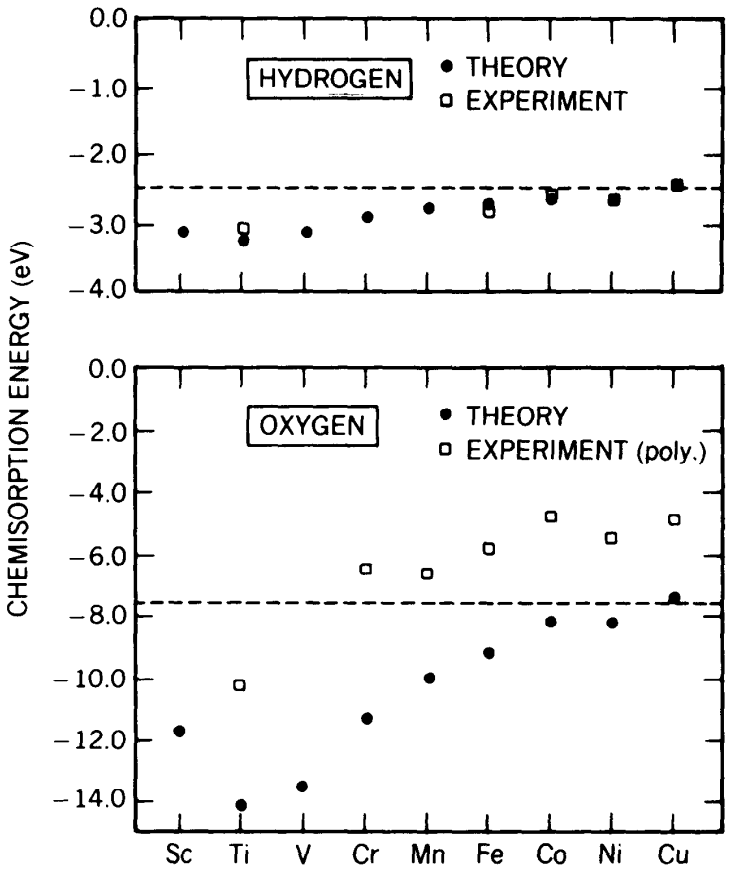

Figure 6.1. Chemisorption energies of hydrogen and oxygen on transition metals across the periodic table that were calculated using the effective-medium theory and also measured on polycrystalline surfaces [23].

It is important to note that the heats of adsorption of oxygen and hydrogen correlate well with the heats of formation of the corresponding oxides and hydrides (per metal atom) as shown by Toyoshima and Somorjai [2] (Figure 6.2). When the heat of adsorption of carbon monoxide is plotted as a function of the heat of formation of the corresponding oxide (per metal atom), two straight lines are obtained (Figure 6.3). The metals that chemisorb less strongly than iron would not readily dissociate CO, whereas those that chemisorb more strongly would dissociate the molecule, as proposed by Joyner and Roberts [3].

6.3 CLUSTER-LIKE BONDING OF MOLECULAR ADSORBATES

When ethylene chemisorbs at ≈ 300 K on the (111) crystal faces of various transition metals (Pt, Rh, Pd), it chemically rearranges to form the molecule–surface compound shown in Figure 6.4. Its structure is determined by LEED–surface crystallography and is very similar to those of the multinuclear organometallic complexes listed in Figure 6.5. The rearranged ethylene, which has also lost a hydrogen, is called *ethylidyne* and belongs to the alkylidyne group (species of the formula C_nH_{2n-1}), a common substituent in surface and in organometallic chemistry (Figures

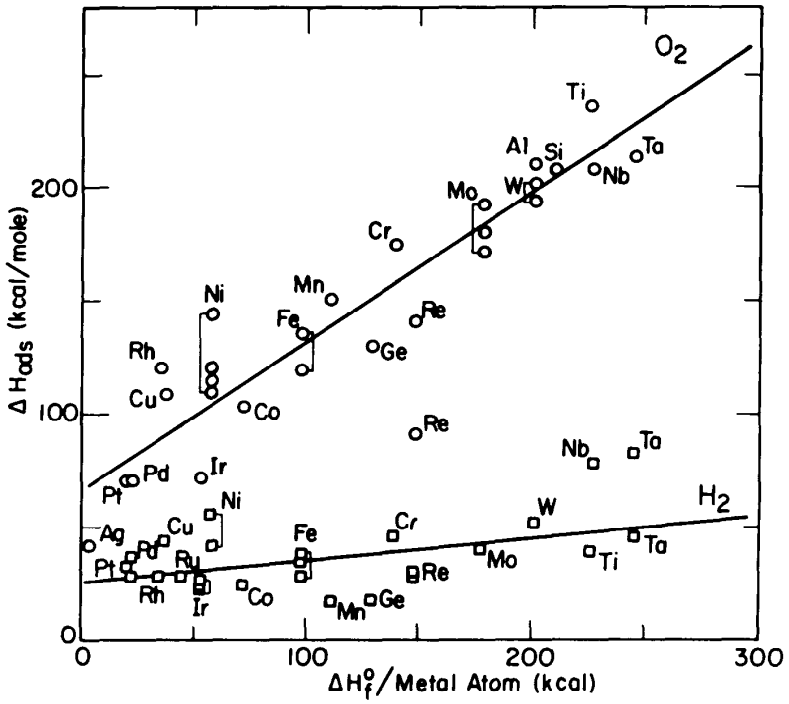

Figure 6.2. Heats of adsorption of O_2 and H_2 on various transition metals as a function of the heats of formation of the corresponding oxides and hydrides (per metal atom) [2].

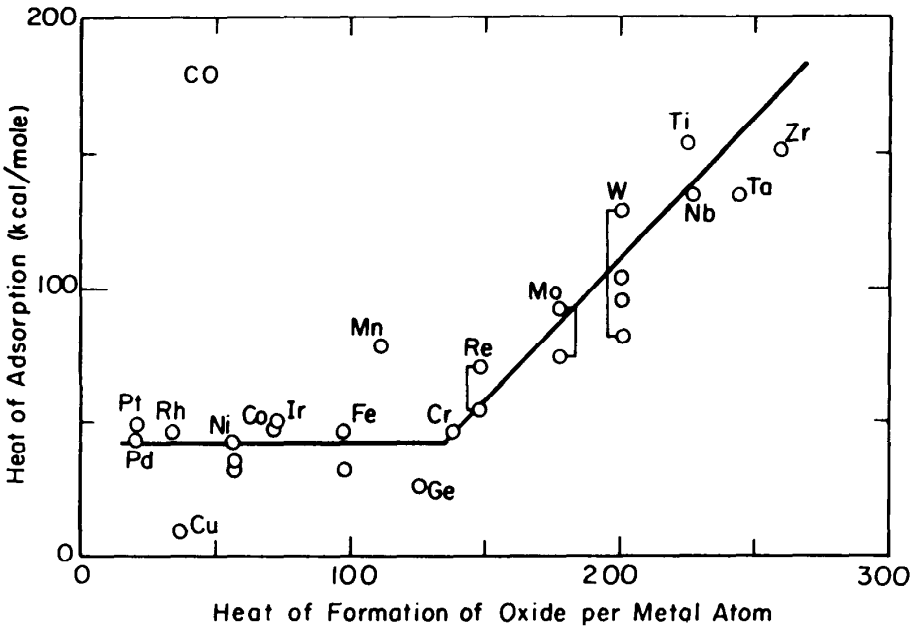

Figure 6.3. Heats of adsorption of CO on various transition metals as a function of the heats of formation of the corresponding oxides (per metal atom) [2].

Different ethylidyne species: bond distances and angles
(r_C = carbon covalent radius; r_M = bulk metal atomic radius)

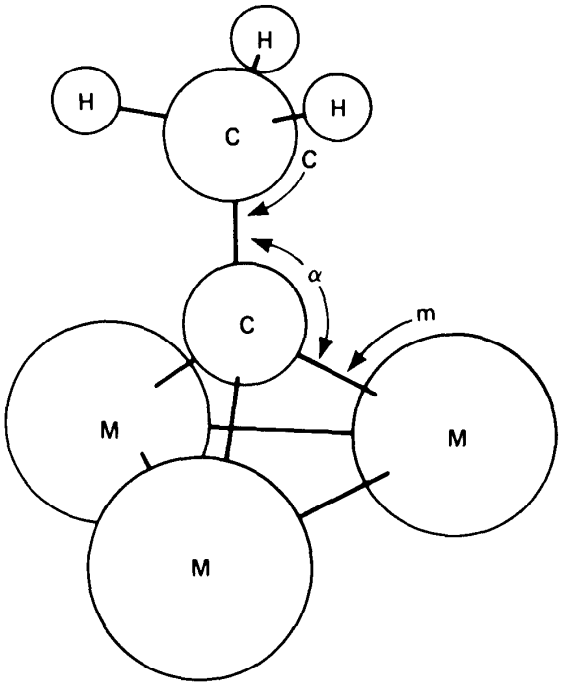

	C [Å]	m	r_M	r_C	α [°]
$Co_3 (CO)_9 CCH_3$	1.53 (3)	1.90 (2)	1.25	0.65	131.3
$H_3 Ru_3 (CO)_9 CCH_3$	1.51 (2)	2.08 (1)	1.34	0.74	128.1
$H_3 Os_3 (CO)_9 CCH_3$	1.51 (2)	2.08 (1)	1.35	0.73	128.1
Pt (111) + (2 X 2) CCH_3	1.50	2.00	1.39	0.61	127.0
Rh (111) + (2 X 2) CCH_3	1.45 (10)	2.03 (7)	1.34	0.69	130.2
$H_3C - CH_3$	1.54			0.77	109.5
$H_2C = CH_2$	1.33			0.68	122.3
$HC \equiv CH$	1.20			0.60	180.0

(*a*)

Figure 6.4. Alkylidyne structure of **(a)** ethylene [24] and **(b)** other alkenes on transition metal surfaces [24] and in **(c)** organometallic clusters [25].

6.4b and 6.4c). The vibrational spectrum of chemisorbed ethylidyne is nearly identical to that in the organometallic cluster which contains three metal atoms (Figure 6.5a). The C—C bond distance is slightly less than the single carbon—carbon bond length of 1.54 Å (0.154 nm), as in the cluster compounds. Thus, the surface chemical bond of chemisorbed ethylene can, as a first approximation, be viewed as a cluster-like bond that contains at least three metal atoms. The C—C bond order

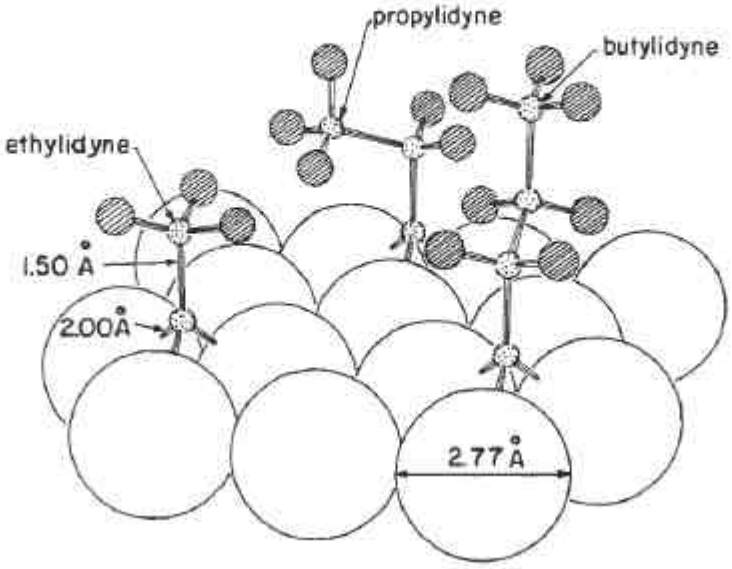

Pt(111) + ethylidyne, propylidyne and butylidyne

(*b*)

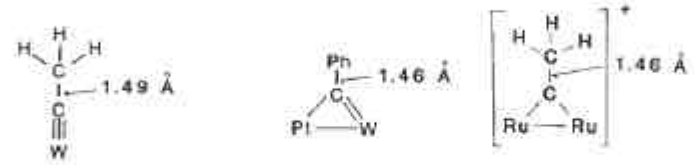

top site bridge bonded

3-fold coordinated 4-fold coordinated "butterfly"

(*c*)

Figure 6.4. *(Continued)*

present in gaseous ethylene is reduced from two to nearly one upon chemisorption. This reduction in bond orders of alkenes and alkynes upon chemisorption on metal surfaces is commonly observed, indicating charge transfer from the molecules into the metal. In fact, the metal work function usually decreases when organic molecules are adsorbed, further proving the direction and magnitude of the charge transfer as the chemisorption bonds form.

There are many chemisorbed organic groups whose surface bonding can be viewed as identical to that of organometallic clusters. Figures 6.5 and 6.6 show the equiv-

Structure			Vibrational Frequencies (cm^{-1})		
Surfaces	Proposed Surface Geometry	Cluster Analogue	Characteristic Dipole-Active Modes	Surface	Cluster
Rh(111) Pt(111) Pd(111) Ru(001) Rh(100)	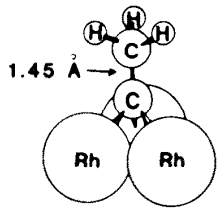	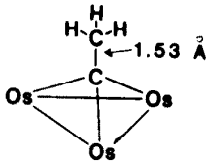	ν_s(MC) ν(CC $\delta_s(CH_3)$ $\nu_s(CH_3)$	435 1121 1337 2880	401 1163 1356 2888
Rh(111) Ru(001) W(110)	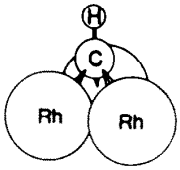	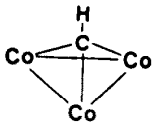	ν_s(MC) ν(CH)	~740 2930	715 3041
gas phase	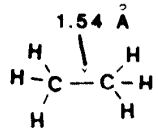		ν(CC) $\delta_s(CH_3)$ $\nu_s(CH_3)$		995 1379 2954

(*a*)

Known Cluster Coordination

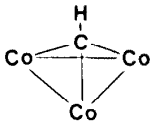

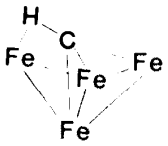

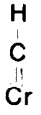

Proposed Surface Geometry on Rh(111)

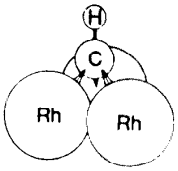

(*b*)

Figure 6.5. **(a)** Vibrational spectra and **(b)** structure of methylidyne on surfaces and in organometallic clusters [25].

Structure			Vibrational Frequencies (cm^{-1})		
Surfaces	Proposed Surface Geometry	Cluster Analogue	Characteristic Dipole-Active Modes	Surface	Cluster
Fe(110) Ni(111) Cu(111) Cu(110)		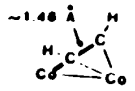	ν(CC)	1402	1302
			ν_s(CH)	3086	2920
Pd(111) Rh(111) Pd(110) Pt(111) Ni(110) Ru(001)			ν(CC)	1301	1260
			ν_s(CH)	2945	2960
Ni(100) Rh(100) Re(001) Pd(100) Fe(111)		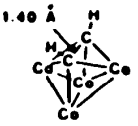	ν(CC)	1120	1199 2991 ---- ----
	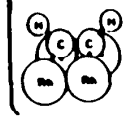	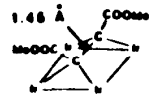	ν_s(CH)	2865	
Pd(111) Rh(111) Ru(001) Pt(111) Ni(110) Ni(111)		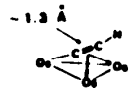	ν(CC)	1534	1380
			ν(CH)	3157	3020
Rh(100)			ν(CC)	----	1305
			ν(CH)	----	3025
gas phase	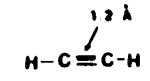		ν(CC)	1974	
			ν_s(CH)	1374	

(*a*)

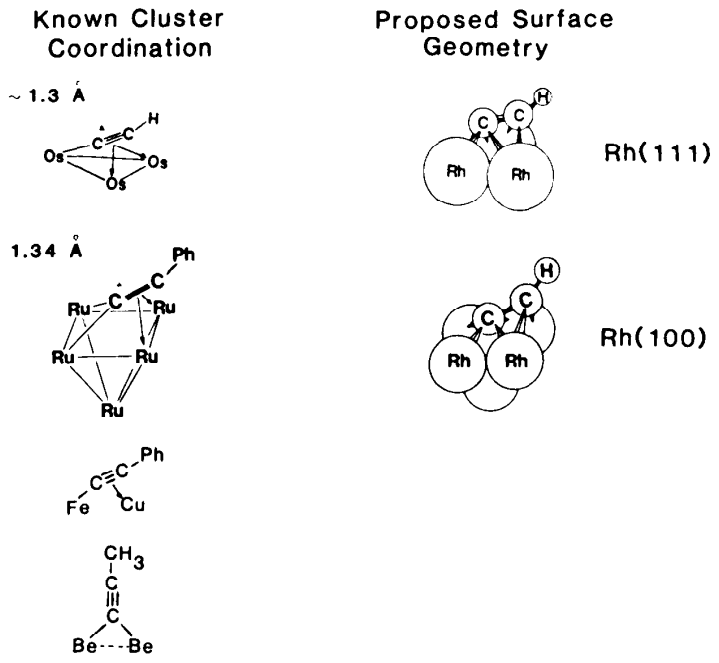

(*b*)

Figure 6.6. **(a)** Vibrational spectra and **(b)** structure of acetylide on surfaces and in organometallic clusters [25].

Structure			Vibrational Frequencies (cm^{-1})		
Surfaces	Proposed Surface Geometry	Cluster Analogue	Characteristic Dipole-Active Modes	Surface	Cluster
Rh(111) + CO	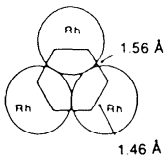	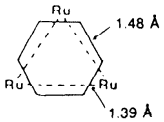	ν_s(CH)	3000	3098
Pt(111) Rh(111)			γ(CH)	776	817
Pd(111) Pd(100)			ν(CC)	1420	1396
Ni(111) Pt(110)					1373
Ni(100) Ni(110)					
gas phase	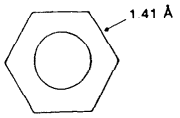		ν_s(CH)	3059	
			γ(CH)	670	
			ν(CC)	1479	

Figure 6.7. Structure and vibrational spectrum of benzene on surfaces and in organometallic clusters [25].

alent bonding arrangements of methylidyne (—CH) and acetylide ($-C_2H$) groups, respectively, on surfaces and in organometallic clusters.

Benzene usually chemisorbs on metals with its ring parallel to the surface (although it may adsorb in a different configuration when it loses hydrogen). Because of charge transfer to the metal, C—C bond elongations occur with respect to the gas-phase configuration, with periodic distortions of the C—C distance that reflect the symmetry of the adsorption site (Figure 6.7). The ring may even bend (see Chapter 2), with two of the opposing carbon atoms closer to the metal surface than the other four carbon atoms. Distortions and elongations of C—C bonds are also found when benzene is bound to clusters of metal atoms in organometallic complexes. Thus the cluster-like bonding model appears to be valid for chemisorbed benzene as well.

The bonding picture of adsorbed molecules becomes more complicated if there are more bonding sites available on the same molecule. For example, pyridine (C_5H_5N) may bind through the lone electron pairs of its nitrogen or through the π electrons of its carbon ring. Thus, depending on the metal, the binding geometry of the substrate, the temperature, or the adsorbate coverage, the molecule may be tilted with respect to the substrate surface, its ring may be parallel with it, or it may be upright with bonding solely through the nitrogen. Partial dehydrogenation can also occur (Figure 6.8).

It is too simplistic to consider that only the nearest-neighbor metal atoms of the substrate participate in the bonding. There is evidence that the atoms at next-nearest-neighbor sites change their location when chemisorption occurs, moving either closer or further away from the chemisorption bonds. This effect will be discussed in Section 6.5.

6.4 THE CARBON MONOXIDE CHEMISORPTION BOND

Carbon monoxide chemisorbed on various transition-metal surfaces is the most intensively studied of all adsorption systems. Thus it provides a model of how surface-science studies, using a combination of techniques, reveal the nature of the surface chemical bond in detail.

For instance, ultraviolet photoemission studies [using 40.8 eV ($\approx 6.5 \times 10^{-18}$ J) photons] compared the energy distribution of photoelectrons from molecular CO, CO chemisorbed on the (100) crystal face of iridium, and iridium carbonyl, $Ir_4(CO)_{12}$ [4]. The spectra reveal the concentration of electrons in the various occupied states. For the CO molecule, these are the 5σ molecular orbital, which has electrons with the lowest binding energy, and the 1π and 4σ orbitals, whose electrons can still be emitted using the applied photon energy. The photoelectron spectra from the chemisorbed CO and from the transition-metal-carbonyl cluster are very similar, indicating that the electron-energy distribution in their chemical bonds is nearly identical (Figure 6.9). Thus the surface chemical bond of CO on iridium is cluster-like. Comparing these spectra to that of molecular CO indicates that the binding energy of the 5σ electrons increases and that these states mix with the 1π states.

The 2π molecular orbitals of gas-phase CO are unoccupied. Molecular-orbital calculations for CO chemisorbed on Ni(100) indicate that the 5σ orbital electrons of CO interact with the $3d_{z^2}$ orbital of nickel and that there is back-donation to the

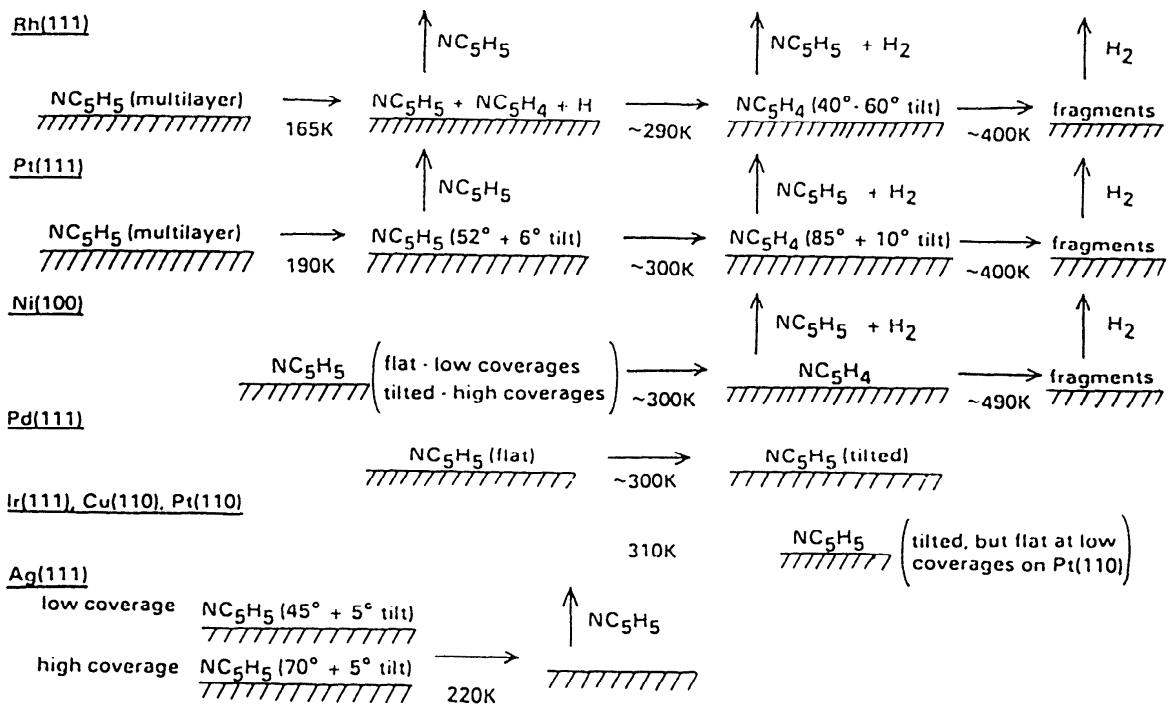

Figure 6.8. Structure and orientation of chemisorbed pyridine as a function of temperature and coverage on different transition metal surfaces [26].

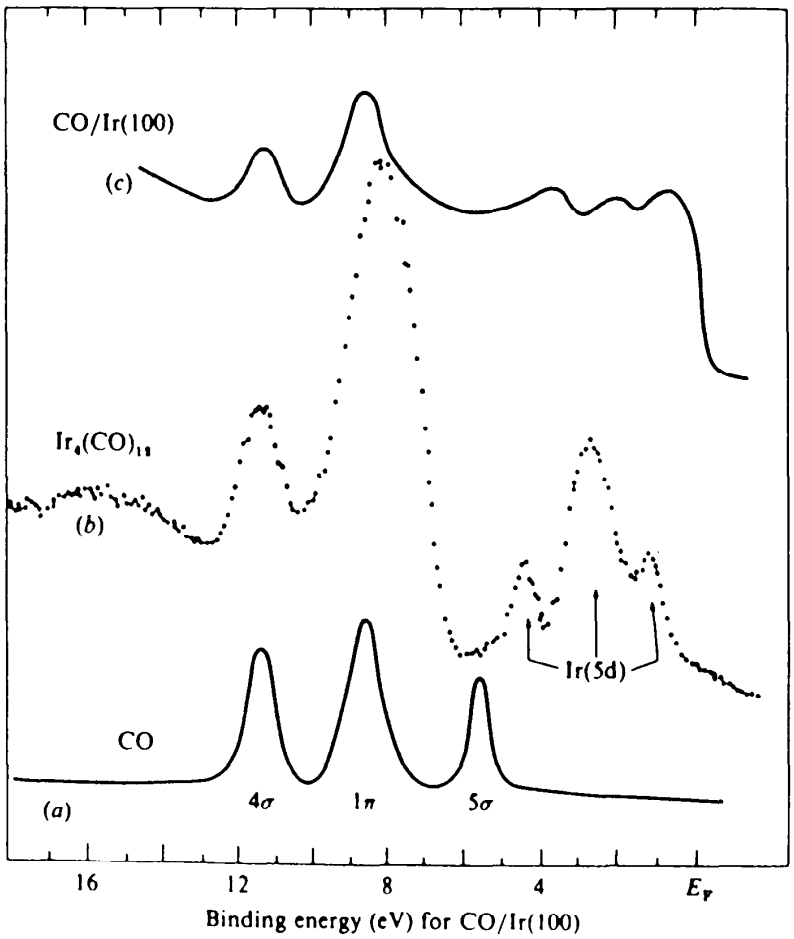

Figure 6.9. Photoelectron spectra [4] of **(a)** CO in the gas phase, **(b)** the $Ir_4(CO)_{12}$ cluster, and **(c)** CO chemisorbed on Ir(100).

antibonding 2π orbital from the filled density of electron states of the metal (Figure 6.10). These calculations have been validated by observed photoelectron spectra. Electron transfer from the filled CO molecular orbitals to the metal and from the metal to the unfilled molecular orbitals explains why the work-function change accompanying CO adsorption on most transition metals is small in magnitude, even though a strong chemisorption bond is produced.

Vibrational-spectroscopy studies indicate that the CO stretching frequency is sensitive to the symmetry of the CO adsorption site (see Table 6.1). Adsorption on a top site leaves CO with a high frequency of vibration, although about 200 cm^{-1} (4×10^{-21} J) lower than in the gas phase. Chemisorption in a threefold site lowers the CO vibration frequency the most, nearly to that of a C—O single bond in an alcohol or ether, for example.

Techniques that are sensitive to the orientation of the chemisorbed molecules (NEXAFS, for example) clearly show that the C=O bond, when chemisorbed on the nickel (100) surface, is perpendicular to that surface.

Higher coverages of CO lead to repulsive interactions between the coadsorbed molecules. These higher coverages (a) lower the average heat of adsorption (as shown in Figure 3.20) and (b) push the CO molecules into new adsorption sites (as shown in Figure 2.31) to maximize the distance between them. When CO is coadsorbed

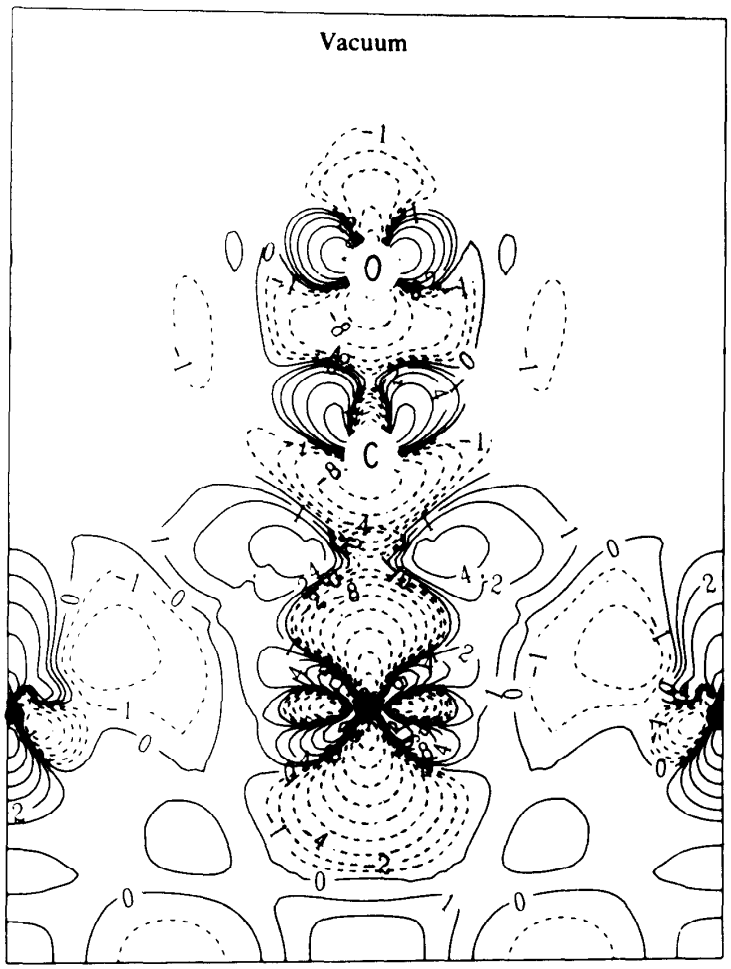

Figure 6.10. Electron density contours of CO chemisorbed on the Ni(100) surface [27].

with benzene, there is an attractive CO—benzene interaction that causes (a) rotation of the benzene molecule with respect to its orientation on the metal surface without CO and (b) relocation of CO into threefold sites that it would not occupy if the benzene were not present.

Coadsorption of CO with alkali metals on transition-metal surfaces increases the heat of adsorption of the molecule.

Thus, coadsorption can change both the strength of the CO chemical bond and its chemisorption site.

6.5 ADSORBATE-INDUCED RESTRUCTURING. THE FLEXIBLE SURFACE

The chemisorption of an atom or a molecule often induces rearrangement of the substrate atoms around the adsorption site. For example, the chemisorption of carbon atoms on the nickel (100) surface occurs at the fourfold site. The nearest-neighbor nickel atoms are displaced away from the carbon, permitting it to move more into the metal surface and bond to the metal atom in the second layer [5, 6]. A small in-plane rotation of the surface nickel atoms around the carbon, shown in Figure

TABLE 6.1. CO-Induced Ordered Structures on Rh(111) Surface

Coadsorbate	LEED Structure	Number of Rh Surface Atoms per Unit Cell	Number of Coadsorbates per Unit Cell	Number of CO Molecules per Unit Cell	C–O Stretching Frequenies (cm^{-1})
—	$(\sqrt{3} \times \sqrt{3})R30°$	3	0	1	2010 (top)
	(2 × 2)	4	0	3	2060 (top) 1855 (bridge)
Ethylidyne ($\equiv CCH_3$)	c(4 × 2)	4	1	1	1790 (hcp hollow)
Propylidyne ($\equiv CCH_2CH_3$)	$(2\sqrt{3} \times 2\sqrt{3})R30°$	12	3	1	1750
Acetylene (C_2H_2)	c(4 × 2)	4	1	1	1725
Fluorobenzene (C_6H_5F)	(3 × 3)	9	1	2	1720
	$c(2\sqrt{3} \times 4)$rect	8	1	1	1670
Benzene (C_6H_6)	(3 × 3)	9	1	2	1700 (hcp hollow[a])
	$c(2\sqrt{3} \times 4)$rect	8	1	1	1655 (hcp hollow)
Sodium (Na)	$(\sqrt{3} \times 7)$rect	14	4	7	1695
	c(4 × 2)	4	1	1	1410

[a]hcp hollow means that one second-layer metal atom lies below the threefold hollow site—in contrast to a fcc hollow, where no second-layer atom lies below the threefold site.

2.18, relieves the stress that would have been caused by the shortened distance between the nearest-neighbor and next-nearest-neighbor metal atoms. This massive local restructuring around the chemisorption site weakens the metal—metal bonds at the surface (an endothermic process). The formation of the strong metal—carbon bonds (an exothermic process) provides the energy needed for the restructuring of the substrate.

Another example of adsorbate-induced restructuring is sulfur chemisorption on the Fe(110) crystal face (Figure 2.19). In this case the nearest-neighbor iron atoms move closer to the sulfur chemisorption site, forming an Fe_4S-like cluster [7]. Again the weakening of the metal—metal bonds nearest to the next-nearest-neighbor bonds is more than offset by the formation of the four strong Fe—S bonds. In Figure 6.11a we show the restructuring of the Cu(110) surface induced by chemisorbed oxygen as monitored by scanning tunneling microscopy (STM).

Chemisorption-induced restructuring can be very well seen using a small metal tip and field ion microscopy. In Figure 6.11b the field ion microscope picture of a rhodium tip is shown when clean and after exposure to carbon monoxide at 420 K at low pressures ($\approx 10^{-4}$ Pa) [8]. The metal tip has been completely reshaped as a result of CO chemisorption. The tip becomes faceted and rougher, the step density is reduced, and extended low-Miller-index terraces are formed.

Rough surfaces that are also chemically active (as will be discussed later) appear to be flexible. The uncovered surface atoms move toward the bulk and to new equilibrium positions. The more open the surface, the larger the movement and the more flexible the surface atoms are. Upon chemisorption these surfaces restructure more readily. It is perhaps instructive to divide surfaces according to their flexibility as shown in Figure 6.12. Close-packed surfaces, like the face-centered cubic (fcc) (111)

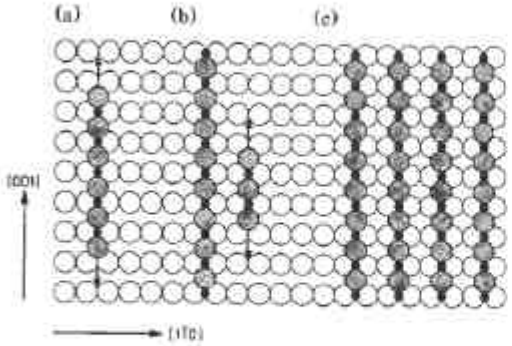

(2x1)-O/Cu(110)

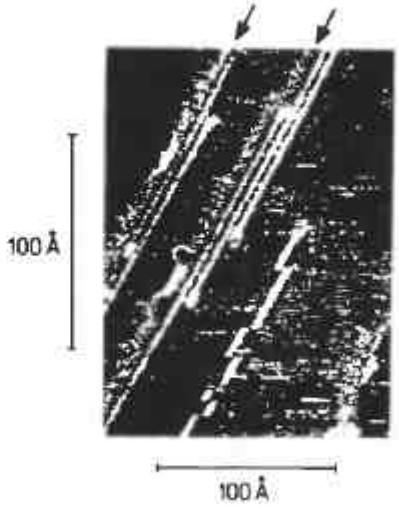

STM image of (2×1)O nuclei in different growth phases: two nuclei two and three rows wide, respectively, at the upper edge of steps along [001] and a single-row nucleus on the flat terrace. Step edges are marked by arrows.

(a)

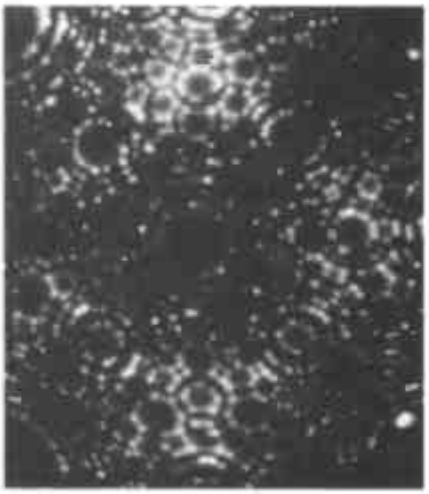

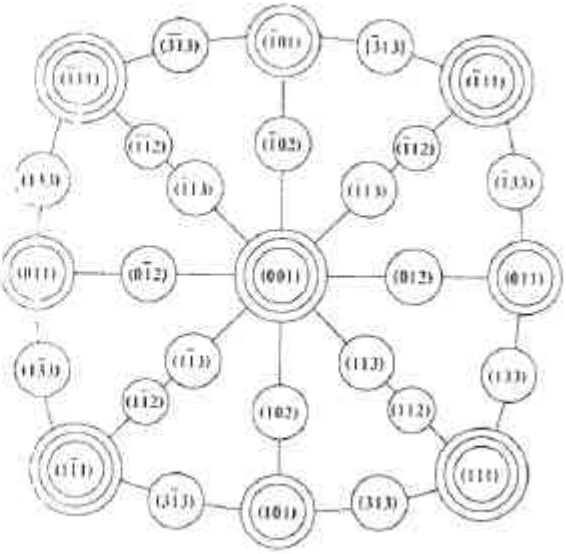

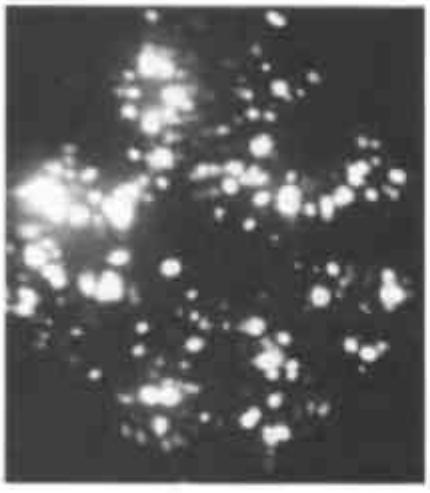

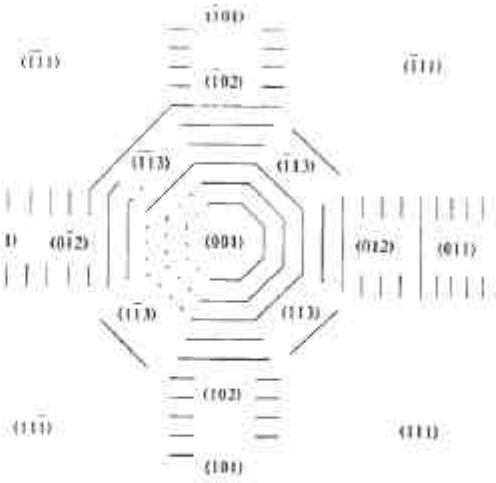

(b)

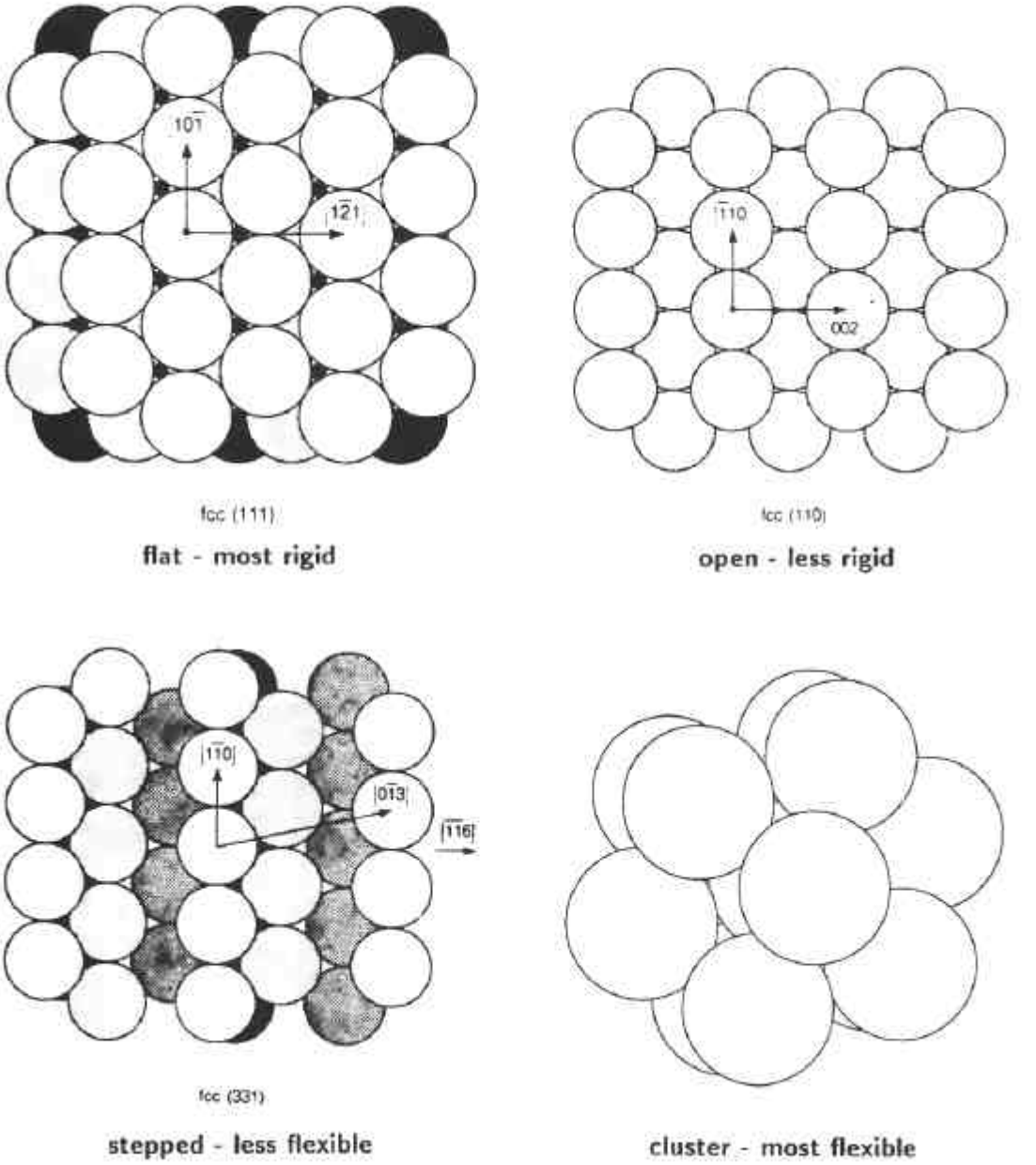

Figure 6.12. Models of surfaces divided according to their atom coordination. Atoms in the close-packed (111) surfaces of fcc metals have the highest coordination, their relaxation is small, and chemisorption-induced restructuring is most difficult. These we call *rigid surfaces*. Clusters have the lowest coordination accompanied by large relaxation and thermodynamically favorable chemisorption-induced restructuring; these are the most flexible. The more open fcc (110) surface and stepped surfaces show intermediate flexibility [29].

Figure 6.11. **(a)** Oxygen-chemisorption-induced restructuring of the Cu(110) surface monitored by scanning tunneling microscopy [28]. **(b)** Field ion micrographs (image gas: Ne; T = 85 K) of a (001)-oriented Rh tip before (*top left*) and after reaction with 10^{-4} Pa CO during 30 min at 420 K (*bottom left*); stereographic projections at the right demonstrate the change in the morphology from nearly hemispherical to polygonal (scheme at the bottom right indicates the coarsening of the crystal and the dissolution of a number of crystallographic planes due to the reaction with CO) [8].

crystal faces are fairly rigid because of the large number of nearest neighbors (high coordination); the atoms stay close to their bulk-like equilibrium positions in spite of the anisotropy of the surface environment. Upon chemisorption these surfaces may restructure; however, the thermodynamic driving force for such restructuring is not large. Clusters of atoms are perhaps the most flexible; the atoms are ready to relocate because of the low coordination of atoms at each surface site. Upon chemisorption, massive restructuring of these clusters may occur because the thermodynamic stability of the chemisorption bonds readily offsets the weakening of the few metal—metal bonds.

Substrate restructuring occurs during the chemisorption of molecules as well. The metal surface atoms that are "relaxed" by moving inward when the surface is clean move outward during the formation of the chemisorption bond. When ethylidyne forms on the platinum (111) surface, in addition to outward movement of the surface atoms, the nearest-neighbor metal atoms move toward the adsorption site, and the next-nearest-neighbor Pt atom moves inward, causing a slight corrugation of the surface, while the Pt atom underneath the adsorption site moves down, away from the carbon atom (Figure 6.13).

Adsorption-induced restructuring can occur on the chemisorption time scale ($\approx 10^{-15}$ sec for charge transfer or $\approx 10^{-12}$ sec for vibrational times). There is evidence, however, that adsorbate-induced restructuring can occur on the time scale of catalytic reactions (seconds). CO oxidation to CO_2 or ammonia reacting with NO to produce N_2 and H_2O show oscillatory behavior under certain circumstances of temperature and reactant partial pressures. The reaction rate alternates periodically be-

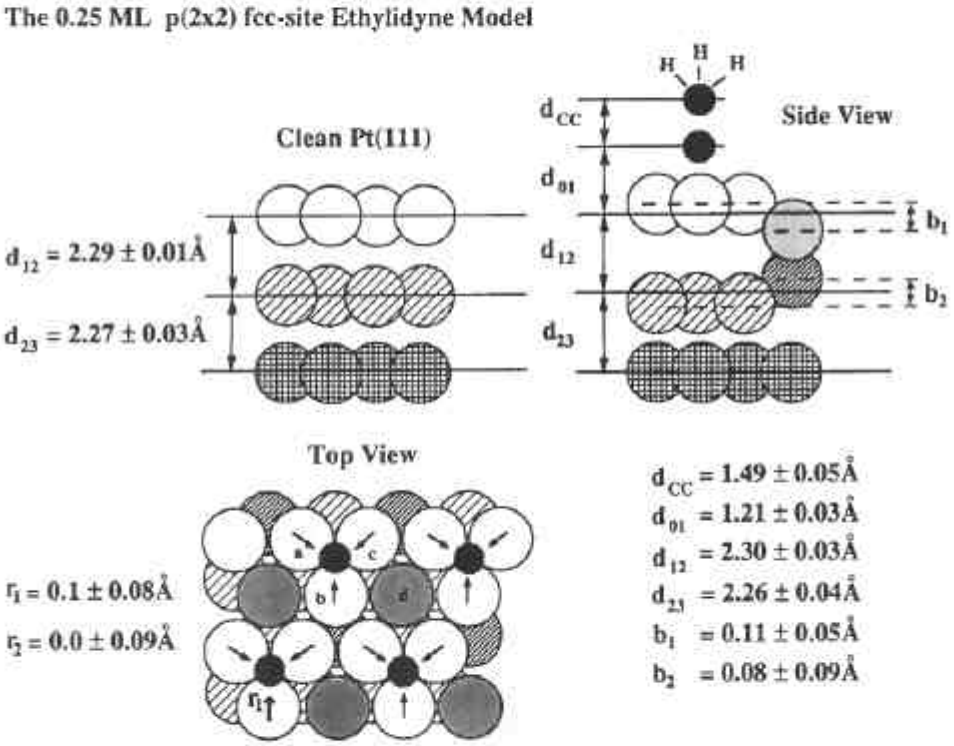

Figure 6.13. Ethylene chemisorption restructures the Pt(111) surface. The Pt atoms move inward around the bonding site, the next-nearest-neighbor metal atom moves downward, and the Rh atom in the second layer moves upward [30].

tween two values. One reason for the oscillation is the periodic restructuring of the surface. In this circumstance the sticking probability of one of the reactants is greater on one type of surface structure, while the sticking probability of the other reactant is greater on the surface structure of the other type. Thus, the reaction rate alternates between the two branches of the reaction, one taking place on the CO-covered or NO-covered metal surface, and the other taking place on the oxygen-covered or ammonia covered metal surface.

Adsorbate-induced restructuring can occur on even longer time scales (hours), involving massive restructuring of the surface by atom transport. For example, sulfur restructures the (111) crystal face of nickel until the metal surface assumes the (100) orientation. Alumina restructures iron through the formation of an iron-aluminate phase to produce (111) crystal faces during ammonia synthesis, regardless of the original crystallite orientation (see Chapter 7). In this circumstance the chemisorption-induced restructuring can be viewed as the initial phase of a solid-state reaction whose kinetics are controlled by atom transport (by diffusion).

Restructuring occurs in order to maximize the bonding and stability of the adsorbate–substrate complex. Thus it is driven by thermodynamic forces and is most likely to occur when the stronger adsorbate–substrate bonds that form compensate for the weakening of bonds between the substrate atoms, an inevitable accompaniment to the chemisorption-induced restructuring process.

6.6 THERMAL ACTIVATION OF BOND BREAKING

When molecules adsorb on a solid surface of low enough temperature (say 20–25 K), they maintain their gas-phase-like structure and remain chemically intact even on the most reactive metal surfaces. As the temperature is increased, either chemical rearrangement of the adsorbed molecule or bond breaking occurs at a certain temperature or narrow temperature range. Each adsorbate–substrate system has a characteristic temperature of bond activation. As the temperature is increased further, another bond-breaking or molecular rearrangement occurs; and sequential bond scission continues at characteristic temperatures until the molecule breaks up into its atomic constituents, which then desorb or diffuse into the bulk. An example, ethylene chemisorption on the platinum (111) surface, is shown in Figure 6.4. The thermal-desorption spectrum indicates sequential hydrogen evolution, while the vibrational spectra taken in the different temperature ranges (Figure 6.14) indicate that molecular rearrangements and chemical bond breaking occur simultaneously, as follows:

$$2C_2H_4(\text{ads}) \xrightarrow{300\text{K}} 2\,-C_2H_3 + H_2\uparrow \xrightarrow{410\text{K}} -C_2H + 2\,-CH + \tfrac{3}{2}H_2\uparrow \xrightarrow{>900\text{K}}$$

$$4C + \tfrac{3}{2}H_2\uparrow$$

In Figure 2.30 the bond-breaking sequences for ethylene and benzene chemisorbed on the Rh(111) surface are compared. At low temperatures the structures of the chemisorbed molecules are different. As the temperature is increased, benzene appears to break into three short-lived acetylene molecules, which become C_2H spe-

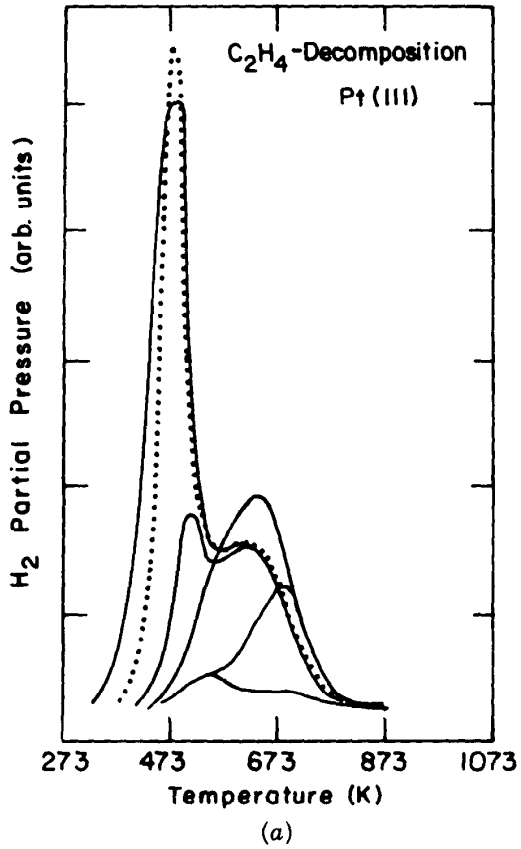

Figure 6.14. **(a)** Temperature-programmed desorption of hydrogen from the thermal decomposition of chemisorbed ethylene on Pt(111) [31]. **(b)** Proposed surface reaction mechanisms to account for the sequential decomposition [32, 33]. Asterisk: denote data taken from reference [33]; daggers denote data taken from reference [32].

cies after hydrogen desorption. At higher temperatures, the molecular fragments produced from ethylene and benzene on the metal surface are the same. The molecular fragmentation sequences for three C_3 hydrocarbons—propadiene, propyne (methylacetylene), and propylene—are shown in Figure 6.15a, and those for *o*- and *p*-xylene are shown in Figure 6.15b.

From the examples above, it is clear that molecular rearrangement or bond breaking on the surface has to be "activated" by increasing the temperature. Perhaps the first experimental observation of this phenomenon was the activated dissociation of dinitrogen (N_2) on iron surfaces, a phenomenon that gave rise to the suggestion of "physisorption" to "chemisorption" transition. Lennard-Jones [9] modeled this transition by a one-dimensional potential-energy curve-crossing diagram that is a simplified reaction coordinate for dissociative chemisorption. A typical diagram is shown in Figure 6.16. By using data from a combination of experiments, one can construct the more complex potential-energy diagram for CO_2 and H_2 formation from CO and H_2O (the so-called water-gas shift reaction) shown in Figure 6.17a or for the dehydrogenation of ethyl amine to acetonitrile in Figure 6.17b.

The molecular mechanisms that give rise to the breakup and reactions of the adsorbate-substrate cluster at a well-defined temperature are not clear, although they

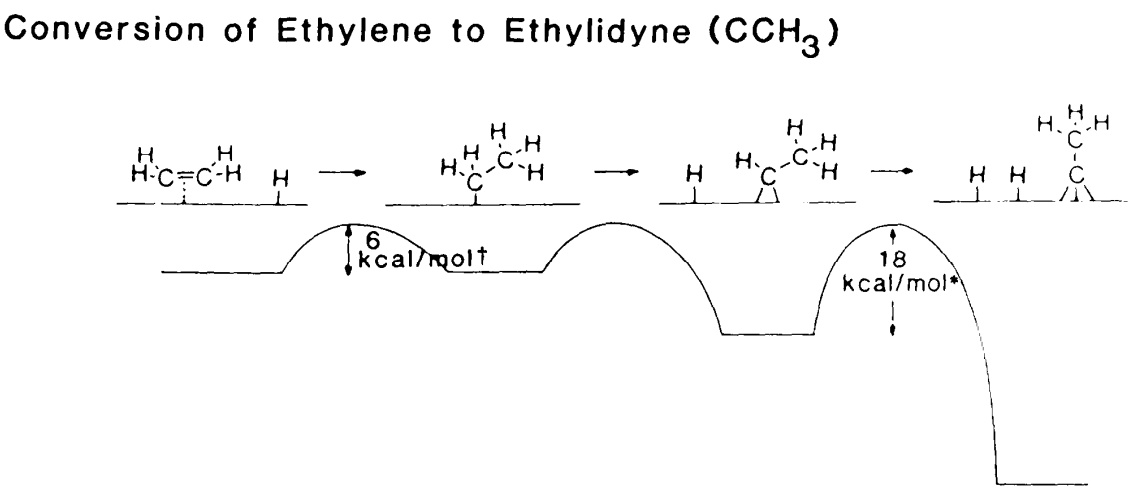

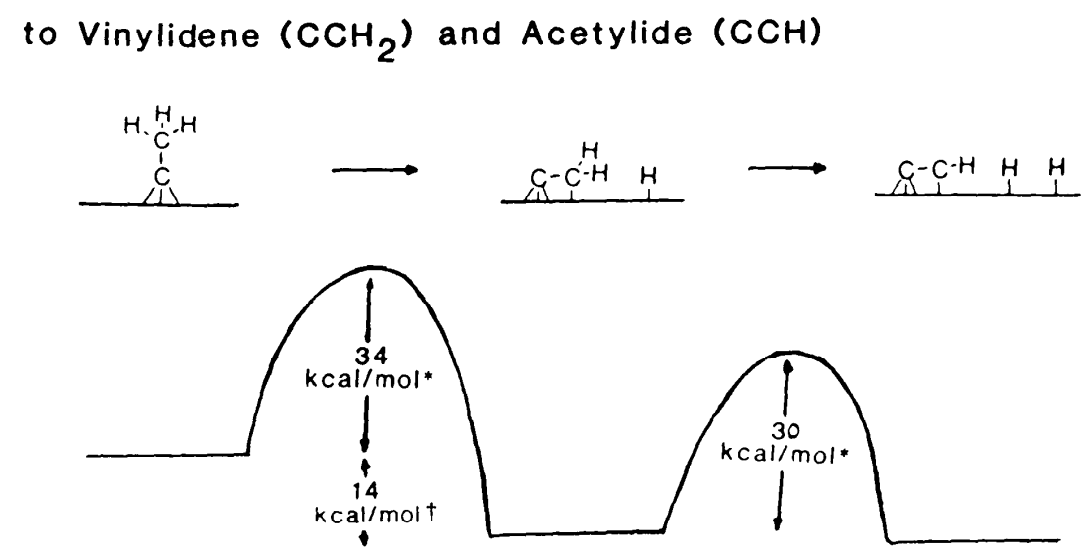

Figure 6.14. (*Continued*)

are a unique property of the surface chemical bond. Nevertheless, their characteristics, dependence on the substrate structure, and adsorbate coverage are well documented and are described below.

6.7 SURFACE-STRUCTURE SENSITIVITY OF BOND BREAKING

Molecules dissociate on more open and atomically rough surfaces at lower temperatures than on flat, close-packed surfaces of low Miller indices. For example, ethylene dissociates on a nickel (111) crystal face at around 250 K (Figure 6.18). On a stepped nickel surface, however, dissociation occurs at below 130 K. Rough surfaces are much more chemically active than flat surfaces at a given temperature. Using a mixed H_2/D_2 molecular beam, the probability of H—H bond breaking was

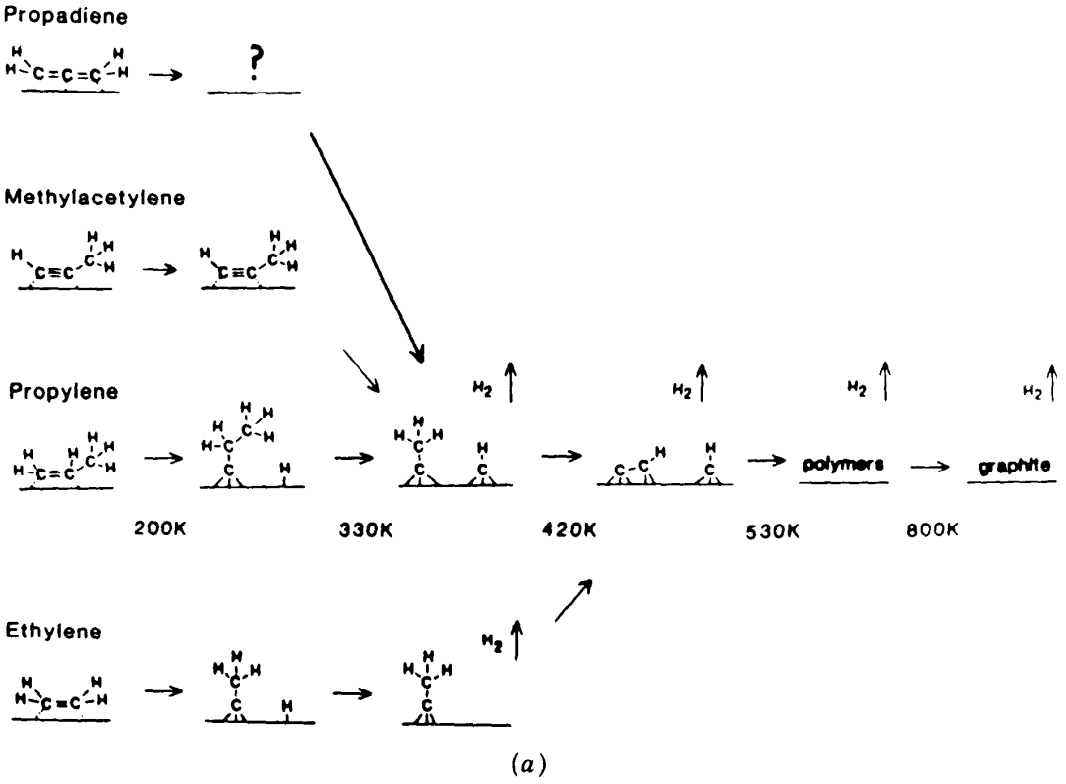

(*a*)

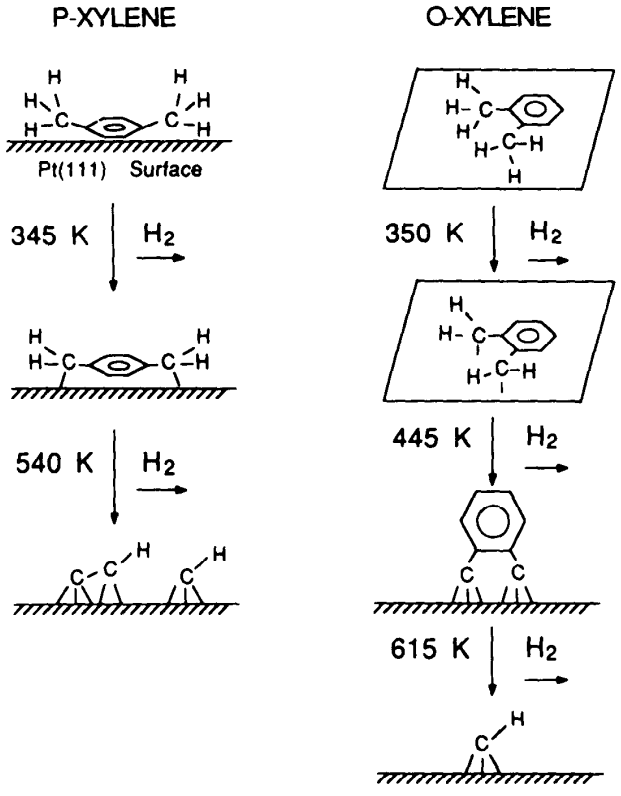

(*b*)

Figure 6.15. **(a)** Thermal fragmentation of C_3 hydrocarbons, propadiene, methylacetylene, propylene. Comparison with ethylene [34]. **(b)** Thermal fragmentation pathways for *p*-xylene and *o*-xylene [35].

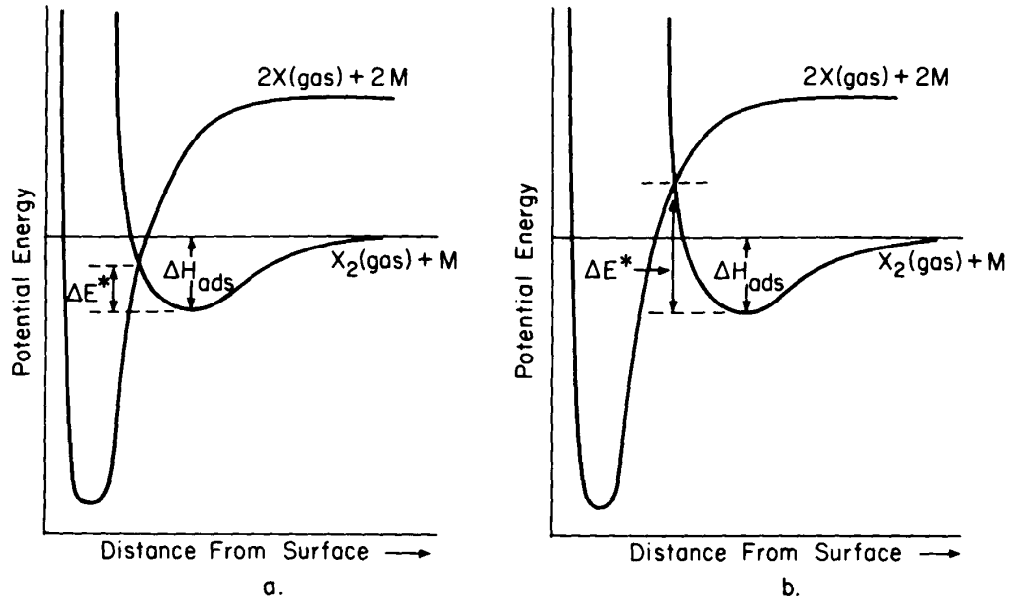

Figure 6.16. One-dimensional potential-energy diagrams showing the possible transition from molecular physisorption to dissociative chemisorption.

studied upon a single collision with a platinum surface by detecting the appearance of HD [10]. On a well-ordered Pt(111) close-packed surface, the reaction probability was below the detection limit of 10^{-3}. On a stepped metal surface, however, the reaction probability was near unity (Chapter 4). Likewise, the dissociative chemisorption of N_2 on the open (111) crystal face of body-centered cubic (bcc) iron was much more probable than on the close-packed (110) crystal face.

Thermal-desorption studies clearly indicate that adsorbed atoms and molecules have higher heats of adsorption at defect sites on the surface. This effect is demonstrated in Figure 4.18, where the thermal desorption of hydrogen is shown for flat, stepped, and kinked crystal faces of platinum. The flat metal surface shows a low-temperature desorption peak. The stepped surface exhibits two desorption peaks; the higher-temperature peak can be readily assigned to desorption from the steps, corresponding to a higher heat of desorption from this site. The kinked surface shows three desorption peaks, with the highest temperature peak corresponding to desorption from the kink sites.

This sensitivity of bonding to surface structure leads to sequential filling of adsorption sites as the coverage is increased, with the sites of highest adsorption energy filling first. This is shown for CO adsorption on a stepped platinum surface in Figure 6.19. At low coverages the step sites are covered with CO because of their high adsorption energy. As the CO coverage is increased, CO fills the terrace sites after all the step sites are covered; two thermal-desorption peaks appear, with the lower-temperature peak indicating the weaker bonding.

Defect sites (steps or kinks) and rough, low-packing-density surfaces have higher charge densities near the Fermi level. This is shown by lower work functions and the higher densities of filled electronic states detected by photoemission studies. These rough surfaces restructure more readily when clean, as described in Chapter 2. They are likely to participate in more massive adsorbate-induced restructuring

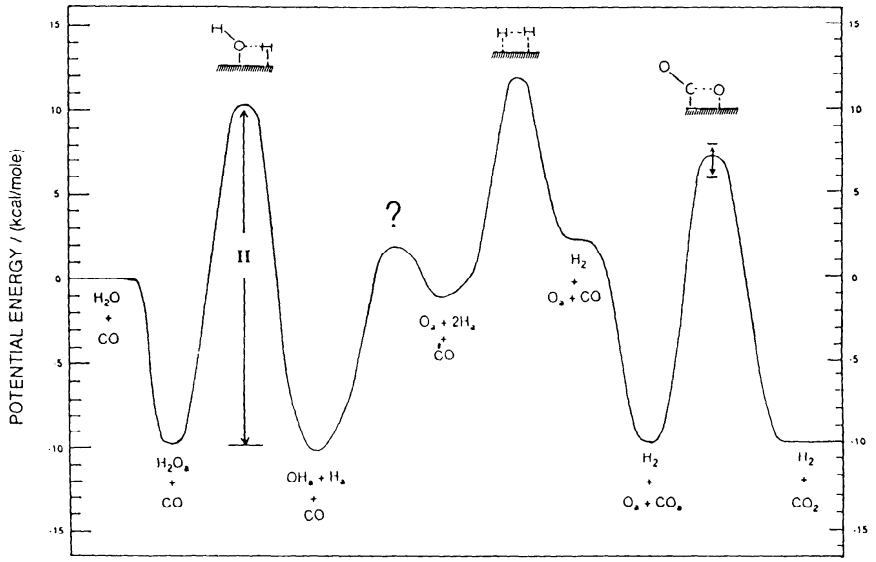
POTENTIAL ENERGY / (kcal/mole)
15
10
5
0
-5
-10
-15
H2O + CO
H2Oa + CO
II
OHa + Ha + CO
?
Oa + 2Ha + CO
H2 + Oa + CO
H2 + Oa + CO2
H2 + CO2
WGS REACTION COORDINATE --->

(a)

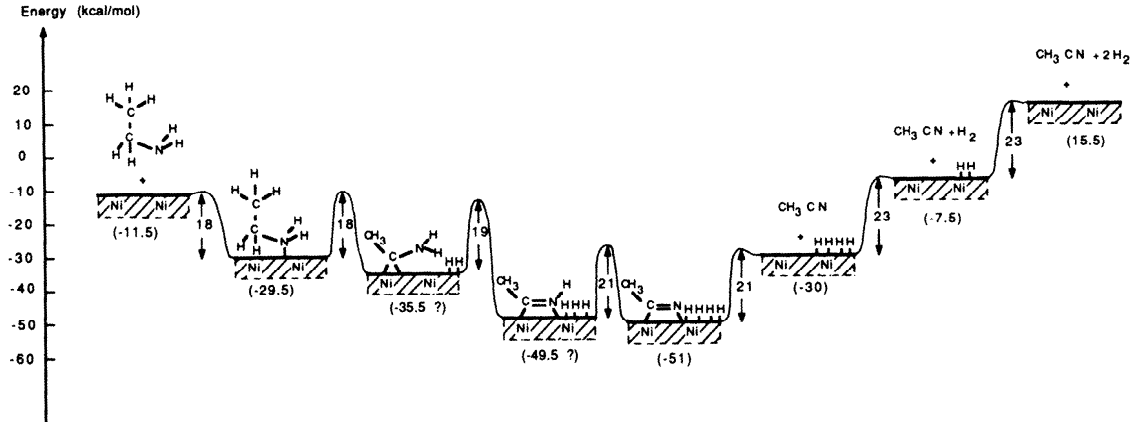

(b)

Figure 6.17. **(a)** Complex potential-energy diagram for the water-gas shift reaction ($H_2O + CO \rightarrow CO_2 + H_2$) on copper surfaces constructed by using the available experimental data [36]. **(b)** Potential energy diagram for the dehydrogenation of ethyl amine to acetontrile on Ni(111) [37].

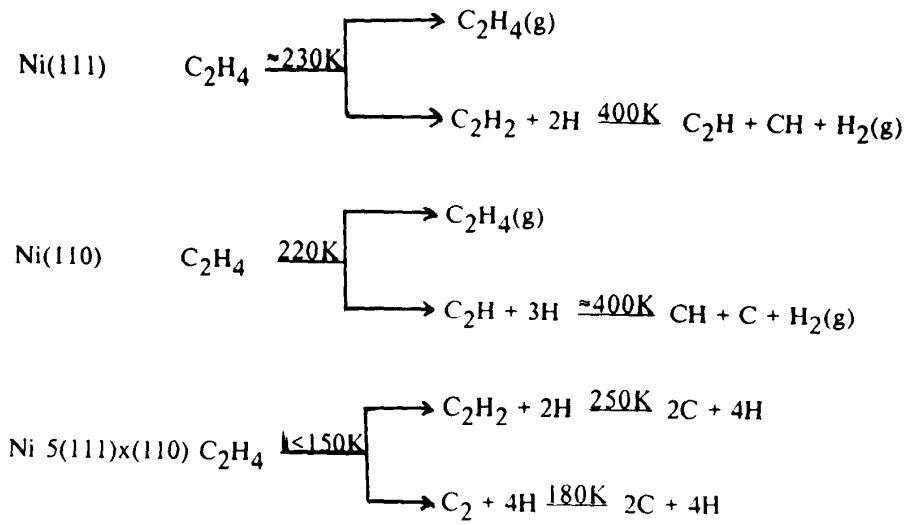

Figure 6.18. Sequential thermal decomposition of ethylene on the (111), the (110), and the stepped 5(111) × (110) crystal faces of nickel. Note the much lower temperature necessary to dissociate the organic molecule on the stepped metal surface [38].

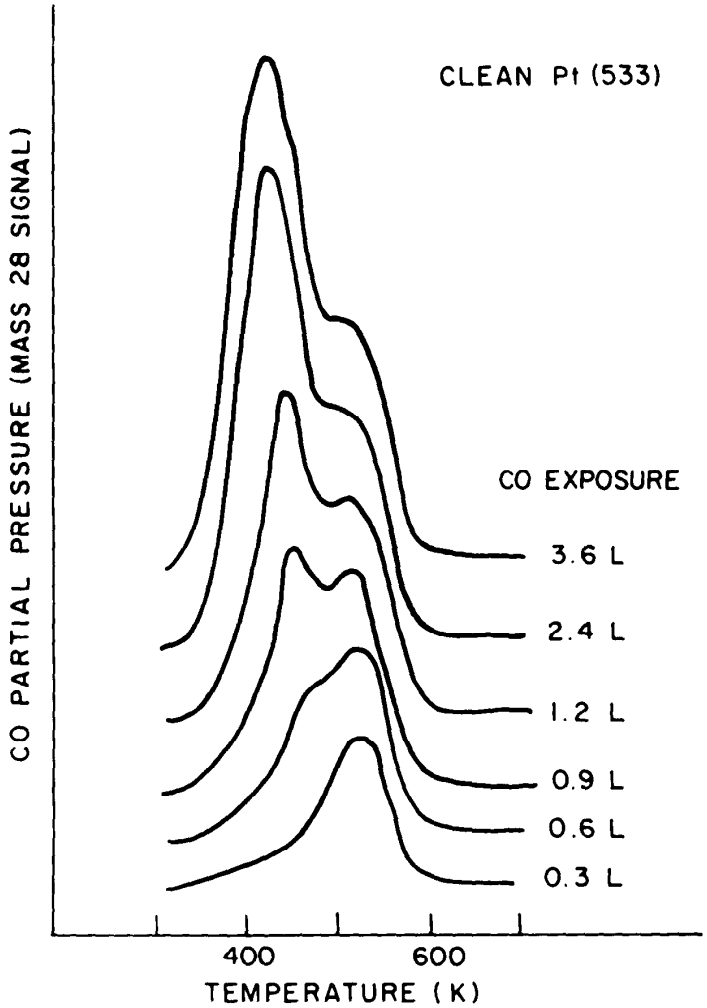

Figure 6.19. Sequential filling of step sites then terrace sites on the stepped Pt(533) surface during CO chemisorption [24].

processes. All these factors can contribute to the enhanced reactivity and bond strength of rough surfaces that lead to the marked surface-structure sensitivity of the adsorbate bond.

6.8 COVERAGE DEPENDENCE OF BONDING AND COADSORPTION

The heat of chemisorption per atom or per molecule declines with increasing coverage for most chemisorption systems. This is shown for potassium on a rhodium (111) crystal face and for CO on a palladium (100) face, respectively, in Figures 6.20 and 3.20b. At low coverages, potassium is strongly bound to the transition metal as it transfers electrons to it to become positively charged. With increasing coverage, adsorbate–adsorbate interaction causes repulsion among the charged species, leading to depolarization and much weakened adsorption bonds until the heat of adsorption becomes equal to the heat of sublimation of metallic potassium. Carbon monoxide chemisorbs with its C—O bond perpendicular to the metal surface, occupying on-top and bridge sites, as shown in Figure 2.31, until about one-half monolayer coverage is reached. The heat of adsorption stays relatively constant with coverage in this coverage range, indicating that very little adsorbate–adsorbate interaction is influencing the bonding of the molecule to the metal. At higher coverages, however, the molecules strongly repel each other, forcing the on-top-site CO molecules to relocate to maximize adsorbate–adsorbate distances (see Figure 2.31), and ΔH_{ads} declines rapidly until it reaches about one-third of its value at low CO coverages.

Thus, increasing coverage of chemisorbed species not only leads to sequential filling of binding sites (the stronger binding sites filling first), as shown in the previous section, but can also weaken the adsorbate–substrate bonds markedly. This effect of coverage influences the surface residence times of adsorbates and subsequently their behavior during chemisorption and surface chemical reactions.

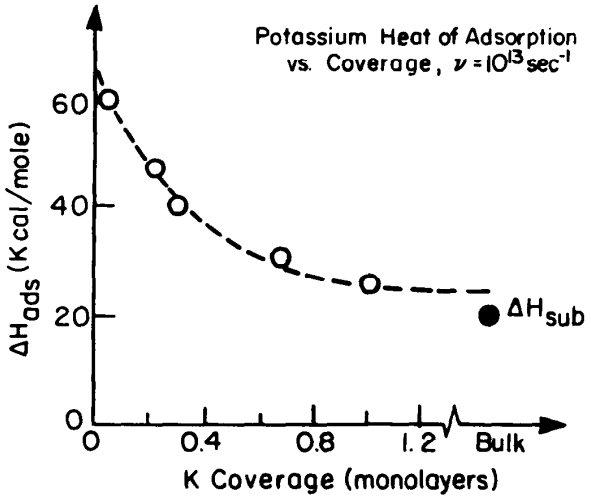

Figure 6.20. Heat of adsorption of potassium on the Rh(111) surface as a function of coverage [39].

6.8.1 Coadsorption

The coadsorption of two different species can lead to either attractive or repulsive adsorbate–adsorbate interaction. The coadsorption of ethylene and carbon monoxide demonstrates the attractive interaction that can occur in the adsorbed layer. CO and C_2H_4 chemisorbed together on the Rh(111) crystal face form the structure shown in Figure 6.21. There are two different molecules per unit cell, indicating attraction among the molecular species of different type. Ethylene adsorption decreases the work function of rhodium (as shown in Figure 6.22), whereas CO increases the work function of rhodium (Figure 6.23) upon chemisorption. Thus, C_2H_4 is an electron donor whereas CO is an electron acceptor on the transition metal, resulting in an attractive donor–acceptor interaction among the two types of adsorbates.

The ordering of one adsorbate by the coadsorption of another through donor–acceptor interaction is commonly observed, as shown for several coadsorbed systems listed in Table 6.1. For Rh(111) the magnitude of the adsorbate–adsorbate attractive interaction is about an order of magnitude weaker [about 4–6 kcal/mole (17–25 kJ/mole)] than most adsorbate–substrate chemisorption bonds [about 30–60 kcal/mole (125–250 kJ/mole)]. Repulsive interaction between two donor or two acceptor coadsorbed molecules leads to separation of the adsorbates by island for-

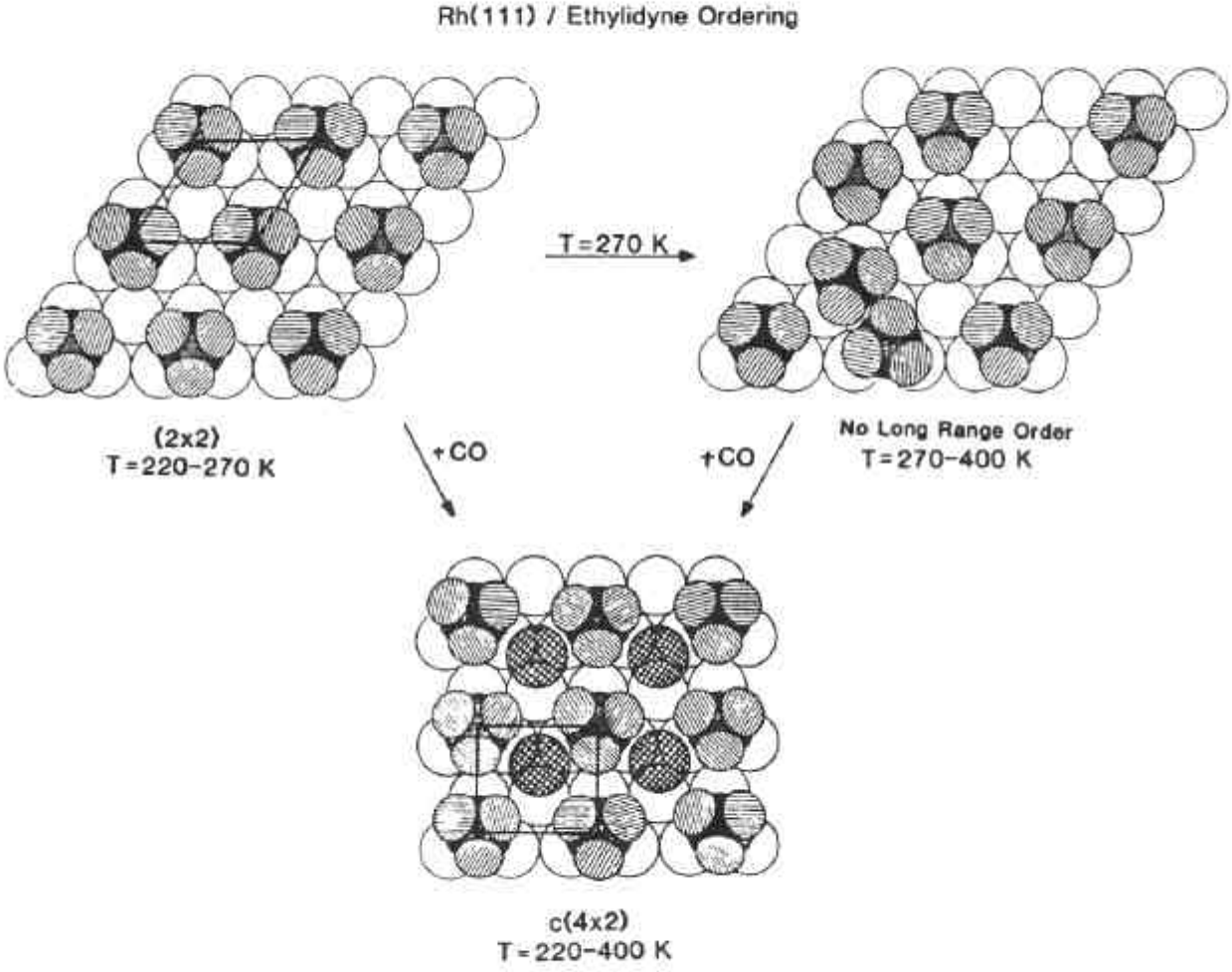

Figure 6.21. Coadsorption of ethylene and carbon monoxide on the Rh(111) surface [25].

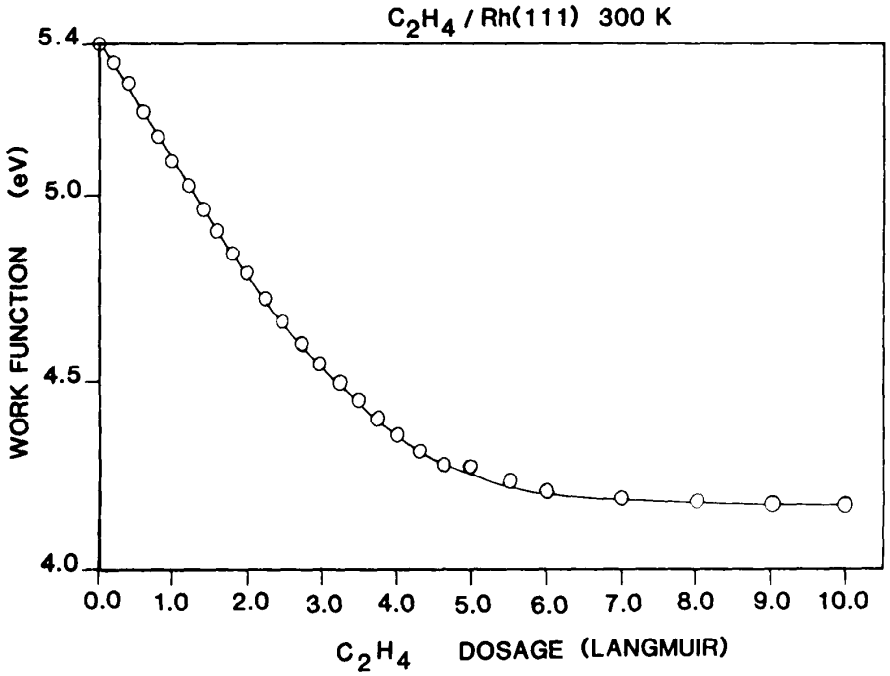

Figure 6.22. Decrease of rhodium work function upon chemisorption of ethylene on the (111) surface [40].

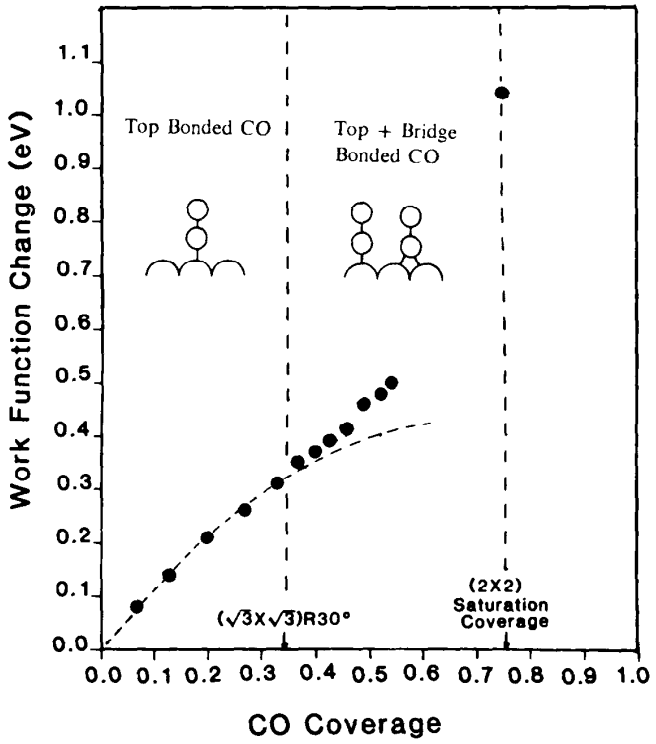

Figure 6.23. Increase of rhodium work function upon chemisorption of carbon monoxide on the (111) surface [40].

TABLE 6.2. Combinations of Adsorbates with Similarly Oriented Dipole Coadsorbed on the Rh(111) Surface

Coadsorbates	LEED Patterns Observed
CO + NO	Disordered or compressed (2 × 2)-3CO [26]
Na + C_2H_2	Disordered
Na + $\equiv CCH_3$	Disordered
Na + C_6H_6	$(\sqrt{3} \times \sqrt{3})R30°$ + $(2\sqrt{3} \times 3)$rect[a]

[a] Because the $(\sqrt{3} \times \sqrt{3})R30°$ and $(2\sqrt{3} \times 3)$rect are observed for Na and benzene, respectively, adosrbed alone on Rh(111), the observation of a mixture of these two LEED structures implies that these two coadsorbates segragate on the surface.

mation or disorder in the adsorbed layer. Several of these systems are listed in Table 6.2.

Strong attractive interaction among adsorbates can lead to dissociation of the molecular species. This is observed during the coadsorption of potassium (donor) and CO (acceptor) on several transition-metal surfaces. Thermal-desorption data indicate CO desorbing at much higher temperatures than normal in the presence of the adsorbed alkali metal, often showing a 17-kcal/mole (71-kJ/mole) increase in its heat of adsorption (Figure 6.24). The CO stretching frequency decreases with increasing dipole moment of coadsorbed donors (Figure 6.25). Isotope-labeling studies (using $^{12}C^{18}O$ and $^{13}C^{16}O$) indicate scrambling of the two isotopic species in the presence

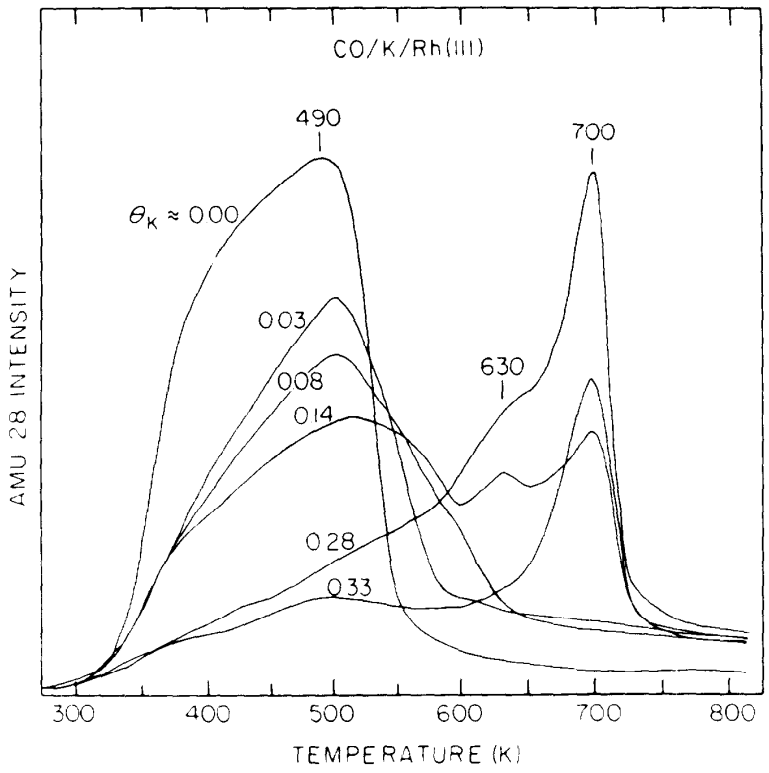

Figure 6.24. Large shift of CO thermal desorption to higher temperature upon potassium coadsorption [41].

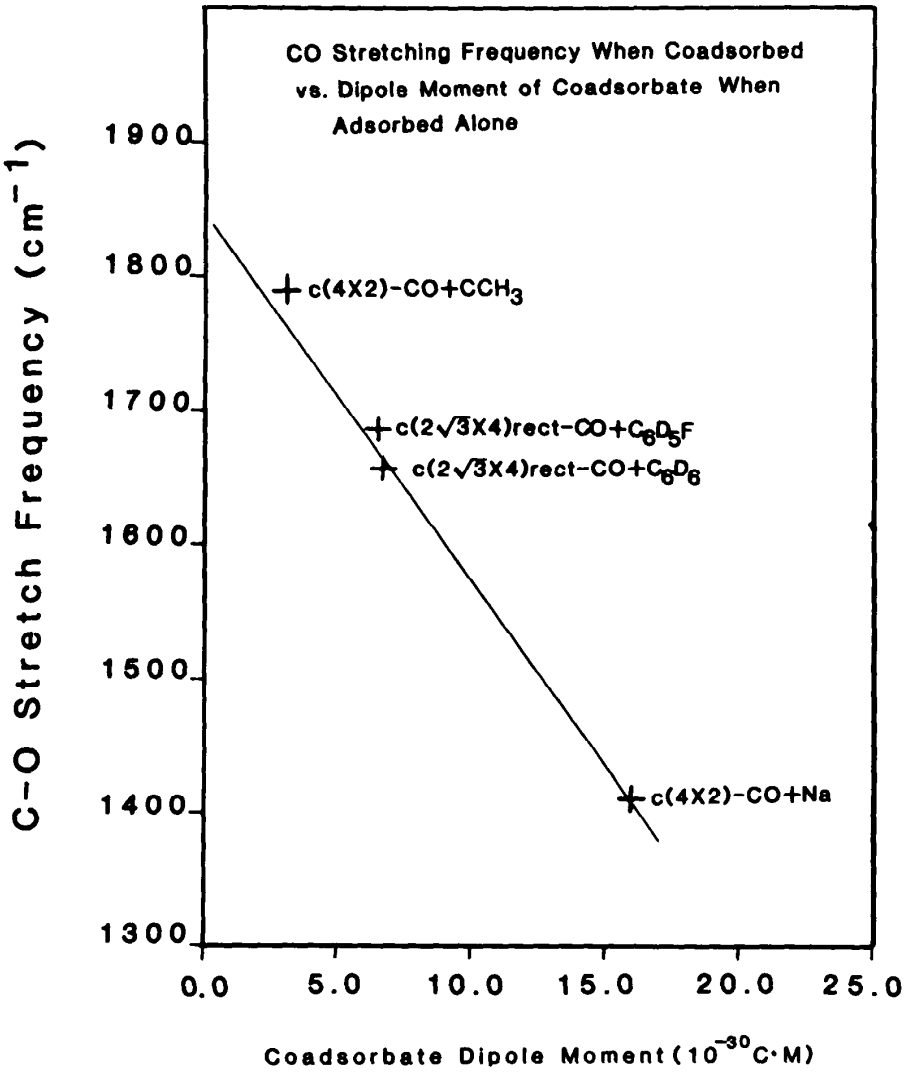

Figure 6.25. Decrease in chemisorbed CO stretching frequency on Rh(111) with increasing dipole movement of coadsorbed donors [40].

of potassium, signaling molecular dissociation, while no dissociation is apparent in the absence of potassium on rhodium. Up to three CO molecules dissociate per potassium atom at an alkali metal coverage of 20% of a monolayer, as shown in Figure 6.26.

Repulsive interaction is also observed with the coadsorption of potassium and ammonia. Both species are electron donors to transition metals. On iron, a 4-kcal/mole (17-kJ/mole) decrease in the heat of chemisorption of NH_3 is observed due to coadsorbed potassium.

Alkali metals are often used as additives during catalytic reactions. They are "bonding modifiers"; that is, they influence the bonding and thus the reactivity of the coadsorbed molecules. Potassium is a promoter in CO hydrogenation reactions where CO dissociation is desired and is one of the elementary reaction steps. The alkali metal also reduces the hydrogen chemisorption capacity of the transition metal. Potassium is a promoter in ammonia synthesis for the opposite reason, because it weakens the NH_3 product molecule bonding to the metal, thereby reducing its sur-

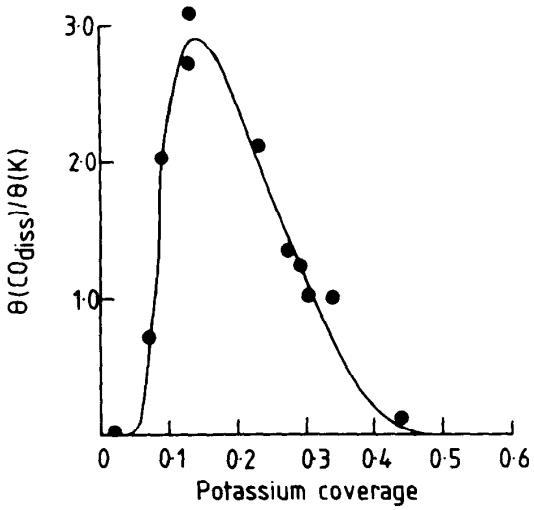

Figure 6.26. Number of CO molecules that dissociate per potassium atom on Rh(111) as a function of potassium coverage [42].

face concentration, which would block important reaction sites. It also aids in the dissociation of dinitrogen (see Chapter 7).

Halogen species can also be important bonding modifiers, because they are powerful electron acceptors. Indeed, they are used as promoters in several catalytic processes (for example, ethylene oxidation to ethylene oxide over silver, or during partial oxidation of methane). Nevertheless, their molecular and atomic chemisorption behavior has been studied less and therefore is not as well understood as the role of coadsorbed alkali-metal ions.

6.9 WEAK SURFACE BONDS

A gas atom or molecule approaching a surface "feels" an attractive potential. The nature of the gas–surface interaction determines the depth of the potential well (it is deep for chemisorption) and the range of the interaction. We may call the adsorbate–surface interaction weak if it leads to heats of adsorption of less than 10 kcal/mole (42 kJ/mole). This usually means that the adsorbate–adsorbate and adsorbate–substrate interactions are of the same order of magnitude. Therefore, the influence of the substrate atomic surface structure on the adsorption site is considerably weaker in this case than it is for chemisorption and more strongly influenced by coverage (i.e., adsorbate–adsorbate interaction).

In the absence of strong attractive interactions induced by charge transfer between adsorbates and surface atoms, weak attractive interactions can be induced in several ways. When a gas atom or molecule with no permanent dipole moment approaches the surface of a metal in which the conduction electrons constitute a mobile, fluctuating electron gas, the surface charge induces a dipole in the approaching species. This attractive induced dipole–surface-charge interaction is similar to that of a gas molecule with a permanent dipole, and the potential energy of interaction is of the form

$$V_{L-J} = -\frac{C}{r^3} \tag{6.1}$$

where C is a constant.

According to the model developed by Lennard-Jones [9] for spherically symmetrical atoms, C is given by $C = mc^2\chi/N_A$, where m is the electronic mass, c is the velocity of light, N_A is Avogadro's number, and χ is the diamagnetic susceptibility of the gas atom. The value of C is on the order of 10^2 kcal·Å^3/mole when r is given in angstroms. In Table 6.3 the surface-interaction energies of several monatomic and diatomic gases are listed at a distance of closest approach of 4 Å (0.4 nm). The interaction potential between metal surfaces and approaching gas atoms has the same range, as given in Eq. 6.1, as was shown by Bardeen [11] and Margenau and Pollard [12], and the constant of proportionality in these cases is of the same magnitude as that derived by Lennard-Jones. It should be noted that, in using these models of gas–surface interactions, the gas atom is assumed to interact with the surface as a whole instead of with individual surface atoms. Recently [13] there has been experimental evidence that in some cases the interaction potential between a metal surface and organic molecules of different types varies inversely as the square of the distance: $V \propto r^{-2}$.

For certain types of gas–surface interactions, it may be useful to view the interaction as between the gas atom and a single surface atom. Weak attractive interaction between a pair of atoms can be due to dispersion forces (London [14, 15]) that represent the interaction of induced fluctuating charge distributions. In addition, molecules that possess permanent dipoles can further polarize each other (Debye [16, 17]) and can have dipole–dipole interactions (Keesom [18, 19]). All these pairwise interaction potentials fall off inversely as the sixth power of the distance.

The dispersion force is due to induced dipole interaction between atoms or molecules through electron density fluctuations. According to London, the potential energy of interaction V_{London} is given by

$$V_{\text{London}} = -\frac{C'}{r^6} \tag{6.2}$$

where, using an approximate model, C' is given by

$$C' = \frac{3h\nu_1\nu_2}{2(\nu_1 + \nu_2)}\alpha_1\alpha_2 \tag{6.3}$$

TABLE 6.3. Values of the Constants of the Lennard-Jones and London Interaction Potentials and the Interaction Energies at the Distance of Closest Approach of 4 Å

	C		C'		V_{L-J}		V_{London}	
Atom or Molecule	(kcal · Å^3/ mole)	(J · nm^3/ mole)	(kcal · Å^6/ mole)	(J · nm^6/ mole)	(kcal/mole) (r = 4 Å)	(kJ/mole) (r = 0.4 nm)	(kcal/mole) (r = 4 Å)	(kJ/mole) (r = 0.4 nm)
$N\theta$	129	539	67	0.280	2.0	8.4	0.016	0.067
Ar	352	1471	802	3.352	5.5	23.0	0.19	0.79
H_2	76	318	176	0.736	1.2	5.0	0.04	0.17
N_2	144	602	919	0.341	2.2	9.2	0.22	0.92
CO_2	362	1513	1872	7.825	5.6	23.4	0.46	1.92

Here α_1 and α_2 are the polarizabilities of the interacting species, ν_1 and ν_2 are their characteristic frequencies of oscillation (oscillator strengths), and h is Planck's constant. The value of C' can be calculated to be on the order of 10^3 kcal Å^6 (4.18 J · nm^6).

Because the values of ν_1 and ν_2 are not easily available, one seeks other ways to estimate the dispersion constant C' from readily measurable molecular properties. One very good approximate expression, which was developed by Slater and Kirkwood [20], can be written as

$$C'\left(\frac{\text{kJ} \cdot \text{nm}^6}{\text{mole}}\right) = 1.52 \times 10^{-3} \frac{\alpha_1 \alpha_2}{\left(\frac{\alpha_1}{n_1}\right)^{1/2} + \left(\frac{\alpha_2}{n_2}\right)^{1/2}} \tag{6.4}$$

where α_1 and α_2 are the polarizabilities in units of Å^3, and n_1 and n_2 are the number of electrons in the outer shells of the molecules. In Table 6.3 the London interaction energies are also listed for a radius of $r = 4$ Å (0.4 nm), along with the dispersion constants for several pairs of like atoms. (For interaction between like species, $\alpha_1 = \alpha_2$ and $n_1 = n_2$.) It can be seen that, due to its short range, V_{London} is a much weaker attractive potential at that distance when compared with the $V \propto r^{-3}$.

Molecules that possess permanent dipole moments can further polarize each other, giving, for the mutual attractive potential energy V_{Debye},

$$V_{\text{Debye}} = -\frac{\alpha_1 \mu_2^2 + \alpha_2 \mu_1^2}{r^6} \tag{6.5}$$

where μ_1 and μ_2 are the dipole moments of the interacting molecules. Direct interaction of two different molecules with permanent dipoles without additional polarization yields

$$V_{\text{Keesom}} = -\frac{2}{3k_B T} \cdot \frac{\mu_1^2 \mu_2^2}{r^6} \tag{6.6}$$

Both V_{Debye} and V_{Keesom} are orientation-averaged expressions, and Eq. 6.6 is restricted to gases in thermal equilibrium. The dispersion interaction V_{London} is appreciably larger than these other two effects (except for the most polar molecules, such as water, for which V_{Keesom} is somewhat larger). Table 6.4 lists the average polarizabilities of several atoms and molecules; Table 6.5 lists the dipole moments of several molecules. There are also many other types of interactions (for example, the ion-induced dipole interaction, which varies as r^{-4}), but they are likely to be less important in gas–surface interactions and will not be discussed here.

It has been shown [21] that the dispersion interaction between pairs of atoms is additive. Calculations show [22] that a large long-range attractive interaction may result from the simultaneous dispersion interaction of many atoms. For example, the attractive potential energy of interaction between two flat plates V in vacuum, due to the summation of the pairwise dispersion forces, varies inversely with the square of the distance: $V \propto r^{-2}$.

TABLE 6.4. Average Polarizabilities for Several Atoms and Molecules

Atom or Molecule	$\bar{\alpha}$ (Å^3)	Atom or Molecule	α (Å^3)
Neon (Ne)	0.39	Hydrogen sulfide (H_2S)	3.78
Argon (Ar)	1.63	Ammonia (NH_3)	2.26
Krypton (Kr)	2.46	Nitrous oxide (N_2O)	3.00
Xenon (Xe)	4.00	Methane (CH_4)	2.60
Hydrogen (H_2)	0.79	Ethane (C_2H_6)	4.47
Nitrogen (N_2)	1.76	Ethylene (C_2H_4)	4.26
Oxygen (O_2)	1.60	Benzene (C_6H_6)	10.32
Carbon monoxide (CO)	1.95	Acetone (CH_3COCH_3)	6.33
Carbon dioxide (CO_2)	2.65		

TABLE 6.5. Dipole Moments of Several Molecules

Molecule	μ (Debye[a])
H_2O	1.84
H_2S	0.89
NO	0.16
CO	0.12
N_2O	0.166
HF	1.91
HCl	1.08
NH_3	1.45
CH_3OH	1.68
CH_3CHO	2.72
$(CH_3)_2CO$	2.9

[a] 1 Debye = 1×10^{-18} esu.

6.9.1 Phase Transformations in the Weakly Adsorbed Layer

A great deal of information can be obtained about the structural changes that occur in weakly adsorbed layers from adsorption-isotherm measurements (amount adsorbed versus pressure). The most commonly studied systems are inert gases adsorbed on graphite or on metal surfaces. At low temperatures the adsorbed atoms form ordered structures (identified by LEED on crystal surfaces), which may be viewed as two-dimensional condensation and evidence of the existence of gas-solid equilibrium. As the temperature is increased, the adsorption isotherm changes. Figure 6.27 shows the adsorption isotherms of krypton on the (0001) crystal face of graphite in the 79.2- to 88.5-K temperature range. The dashed line indicates the possible phase diagram. At around 85 K there is a first-order phase transformation that is associated with the onset of disorder in the adsorbed monolayer, indicating the formation of a liquid-like film. Above this temperature, therefore, a solid-liquid equilibrium exists.

When the coverage increases at a given temperature (one that is below the temperature at which the liquid-like film forms), the surface structure of the adsorbed atoms changes due to repulsive adsorbate-adsorbate interactions. This effect is also

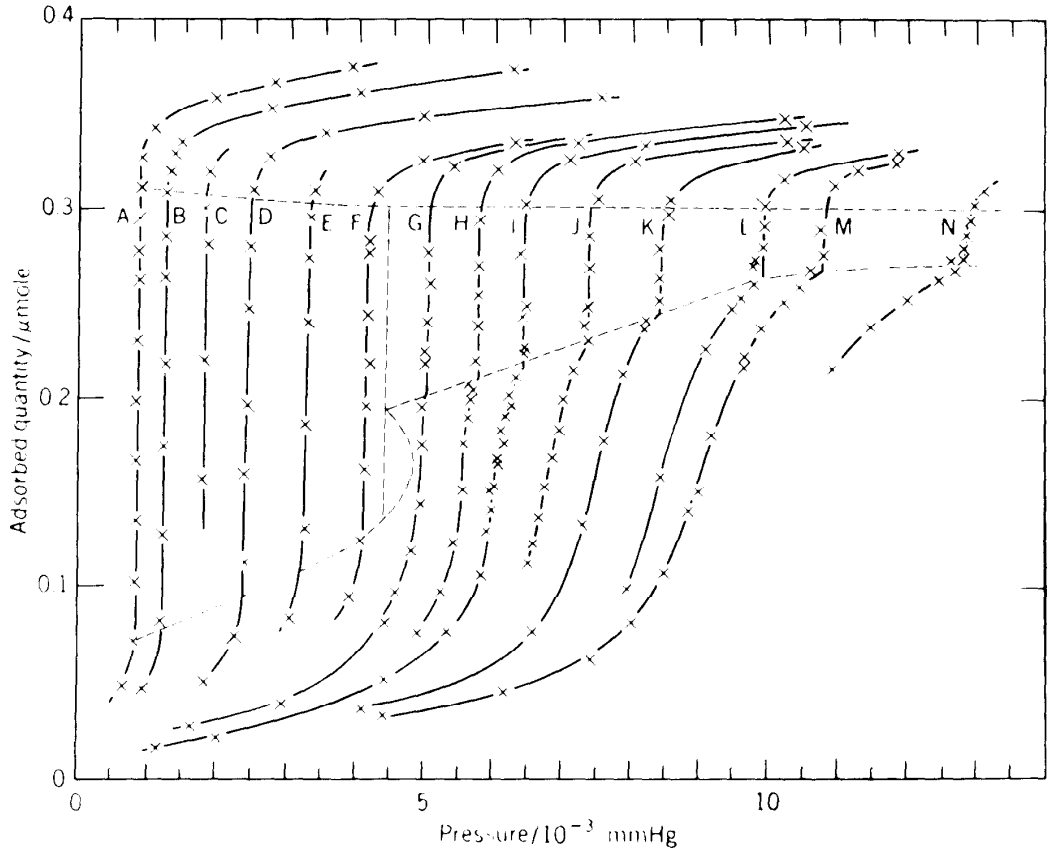

Figure 6.27. The adsorption isotherms of krypton on the (0001) graphite surface in the 79.2- to 88.5-K temperature range: A, 79.24; B, 80.54; C, 81.77; D, 82.83; E, 83.84; F, 84.69; G, 85.33; H, 85.74; I, 86.12; J, 86.58; K, 87.08; L, 87.61; M, 87.81; N, 88.46 K [43].

implied by the rapid decline of the heat of adsorption with increasing coverage, as shown for several weakly adsorbed systems in Figure 6.28. Incommensurate surface structures usually form because the substrate structure (periodicity) has little influence on the ordering behavior of these systems. At low enough temperatures, multilayers can be produced, and their properties (number of layers, heats of interaction between the layers) can be analyzed using the BET isotherm analysis (see Chapter 3).

Total surface-area measurements are a useful application of weakly adsorbed monolayers, because their interaction energies are largely independent of the chemical composition of the substrates. Gas separation is another application of weak adsorption. Oxygen (O_2) and nitrogen (N_2) can be separated from air by selective adsorption, because the polarizability of N_2 and therefore its heat of adsorption is greater than that of O_2. The gas chromatograph operates on the principle of small differences in heats of adsorption of molecules. The difference changes the residence times of adsorbates (called *retention times* in this circumstance) on a column, thus separating them by delaying their arrival at the detector. Separation of macromolecules can be achieved at the solid–liquid interface (liquid-phase chromatography), where the diffusion rates of different molecules are influenced by their somewhat different binding at the interface.

Weakly adsorbing surfaces can be prepared that either preferentially adsorb (hydrophilic interface) or repel (hydrophobic) water. Hydroxylated silica surfaces and

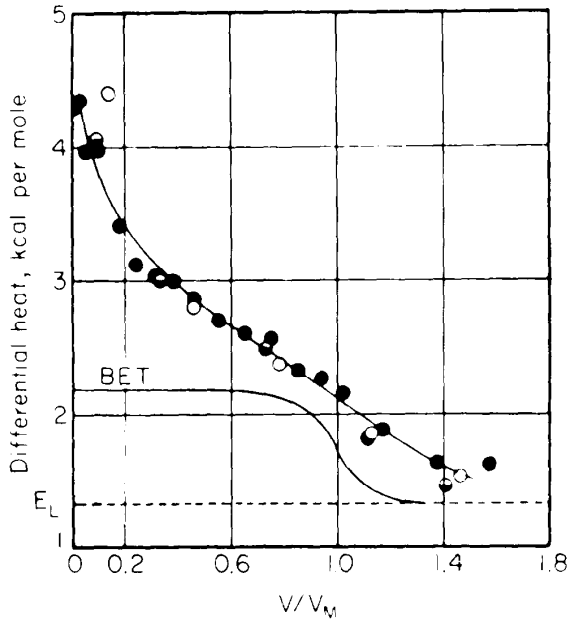

Figure 6.28. Differential heat of adsorption of nitrogen on carbon black at 78.5 K [44].

fluorocarbons behave in this way, respectively, and high-surface-area molecular sieves have been developed with these properties. Such interfaces can be used to separate organic and aqueous phases of solutions.

Weakly adsorbing insulator or semiconductor surfaces that operate by charge transfer (such as SnO_2, as shown in Chapter 5) can be used as detectors or for

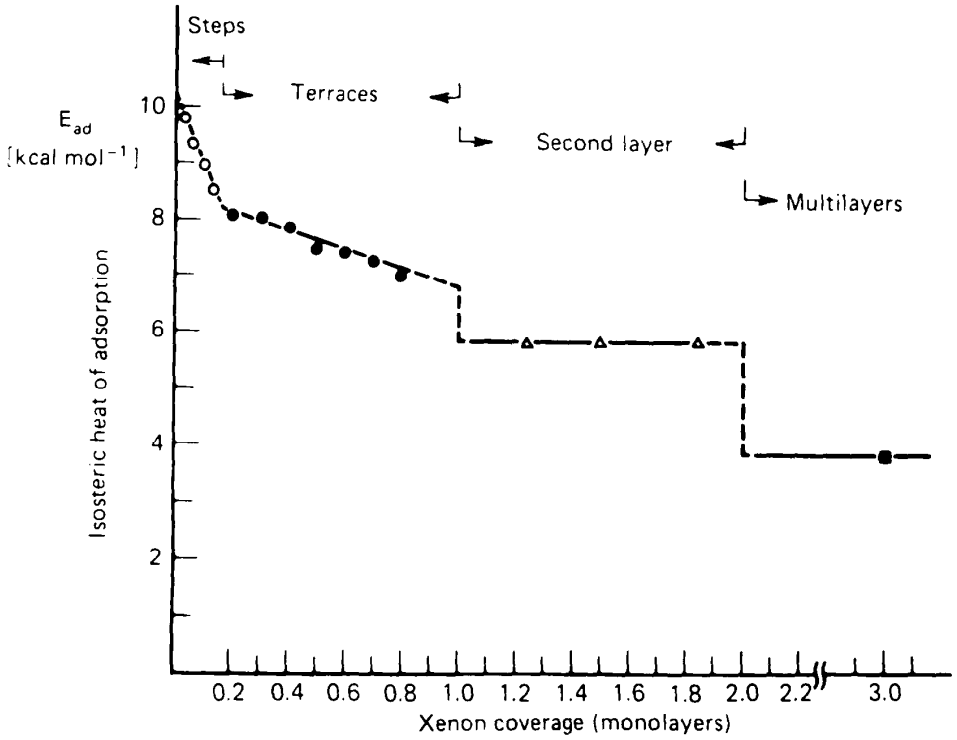

Figure 6.29. Heat of xenon adsorption on the stepped palladium 8(100) × (110) surface as a function of coverage [45].

separating gases. Their principles of operation are different from those of surfaces that form polarizability bonds, because they respond to small differences in ionization potentials or electron affinities.

The adsorption of even weakly bound atoms shows variations due to the structure of transition metals. Xenon exhibits easily detectable changes in heat of adsorption on palladium crystal surfaces (as shown in Figure 6.29), depending on location (at a step site or on a terrace site). The higher heat of adsorption at the terrace sites is not surprising, since the lower work function at defect sites indicates larger electric fields at these sites, thus influencing the bonding of the highly polarizable xenon atom. The weak adsorption of the chemically passive xenon can then be used to learn about the atomic heterogeneity of the metal surface structure in a noninvasive manner, using relatively simple thermal desorption studies. As Figure 6.29 indicates, there are differences in the heat of adsorption of xenon in the first and second monolayers, and even between the second layer and the multilayers that adsorb over it. Thus, the effect of weak polarizability bonding at the metal surface can influence the bonding of at least two layers of adsorbates.

6.10 SUMMARY AND CONCEPTS

- The formation of the surface chemical bond is accompanied by charge redistribution in the adsorbate and the substrate that may also change the structures of both.
- Bond energies for a given atom or molecule adsorbed on transition metals increase from right to left in the periodic table.
- Molecular adsorbates exhibit bonding and structure that are similar to those in cluster compounds (multinuclear organometallic clusters, for example).
- The adsorbate bond is surface-structure-sensitive, and adsorbate-induced surface restructuring frequently occurs. Rough surfaces (with lower atomic coordination) restructure more readily.
- Bond breaking in adsorbates requires thermal activation and usually occurs in several steps at well-defined temperatures with increasing temperature.
- Changes of coverage and coadsorption have marked influence on the bonding, location, and orientation of adsorbates.
- Weak surface bonds play important roles in gas chromatography separation of molecular mixtures and in gas separation and detection.

6.11 PROBLEMS

**6.1 Ethylidyne restructures the Rh(111) crystal face [30], sulfur restructures the Fe(110) face [7], and carbon restructures the Ni(100) face [6, 46]. The surface metal atoms move into new equilibrium positions upon chemisorption in different ways, and there is evidence of restructuring even in the second substrate layer under the surface. Review the available data and point out the important electronic and structural parameters that influence the nature and magnitude of chemisorption-induced surface restructuring.

**6.2 Adsorbate-induced restructuring of surfaces could explain the formation of cluster-like bonding of adsorbates on metal surfaces. Discuss how the strength of the chemisorption bond is likely to influence the restructuring of metal surfaces.

**6.3 One of the unique features of the surface chemical bond is how sequential bond breaking occurs in the adsorbed monolayer as the temperature increases. Find two examples in the surface-science literature for the thermal activation of bond scission. Describe how sharp the transition is (its temperature range), its substrate structure dependence, and its coverage dependence. Speculate on the reasons for breaking 400-kJ/mole chemical bonds by merely increasing the temperature a few degrees in a given temperature range.

**6.4 The heat of adsorption of CO is determined as a function of coverage by several research groups using single-crystal metal surfaces [47]. Review and describe the experimental procedures of how such experiments are carried out.

**6.5 Surface defects, steps, and kinks dissociate molecular bonds more readily and exhibit higher heats of adsorption for the chemisorbed atoms or the molecular fragments. Find two examples of such chemical behavior and discuss the possible relationship between the electronic structure and the atomic structure of the defect and its reactivity to break adsorbate bonds.

**6.6 Low-energy electron diffraction studies of rare gases on copper have detected several ordered surface structures that form as a function of coverage [48, 49]. Explain how changes in bonding give rise to alterations of surface structure and the two-dimensional phase diagram that has been constructed.

**6.7 The binding energy of potassium is strongly coverage-dependent. When it is coadsorbed with CO, it markedly strengthens the CO bond to the transition-metal substrate. When it is coadsorbed with ammonia, it decreases the heat of adsorption of the molecule on iron surfaces. Explain the reasons for these intriguing properties [50–52] of adsorbed potassium for altering the chemical bonding in the monolayer.

**6.8 Inert gases decrease the work function of transition metals [53–55]. Although their bonding is weak, they exhibit detectable surface-structure sensitivity. This has been particularly well demonstrated for the adsorption of xenon. Review the available literature and discuss the nature of inert gas bonding to metal substrates that gives rise to these effects.

**6.9 The adsorption isotherm of xenon on graphite has been measured at different temperatures [56–60]. Review the experimental results and discuss the surface phases of xenon that were detected. Would you expect krypton to behave similarly on the same substrate? Explain.

**6.10 When ethylene chemisorbs on the (111) face of rhodium, it lies with its C=C bond parallel to the surface at low temperatures, forms ethylidyne (C_2H_3-) at 300 K, and dissociates to C_2H- and $CH-$ groups at 410

K. Find organometallic multinuclear cluster compounds with similar organic species attached and discuss their bonding behavior (bond distances, binding sites, and bond angles) [61].

**6.11 The heat of adsorption of carbon monoxide varies across the periodic table. There is a great deal of data available to demonstrate this, especially for transition metals [47]. The heat of adsorption per CO molecule also varies markedly with coverage, especially above one-half monolayer for most metals. CO may also occupy top, bridge, threefold, and other sites where its binding energy is different at each site. Review the available data, discuss the trends, and comment on the effects of the changing electronic structure of the substrate and the variation of the atomic structure of a given substrate on the binding of CO.

REFERENCES

[1] J.K. Nørskov. Covalent Effects in the Effective-Medium Theory of Chemical Binding: Hydrogen Heats of Solution in the 3*d* Metals. *Phys. Rev. B* **26**:2875 (1982).

[2] I. Toyoshima and G.A. Somorjai. Heats of Chemisorption of O_2, H_2, CO, CO_2, and N_2, on Polycrystalline and Single Crystal Transition Metal Surfaces. *Catal. Rev. Sci. Eng.* **19**:105 (1979).

[3] R.W. Joyner and M.W. Roberts. Auger Electron Spectroscopy Studies of Clean Polycrystalline Gold and the Adsorption of Mercury on Gold. *J. Chem. Soc. Faraday Trans. I* **69**:1242 (1973).

[4] E.W. Plummer, W.R. Salaneck, and J.S. Miller. Photoelectron Spectra of Transition-Metal Carbonyl Complexes: Comparison with the Spectra of Adsorbed CO. *Phys. Rev. B* **18**:1673 (1978).

[5] Y. Gauthier, R. Baudoing-Savois, K. Heinz, and H. Landskron. Structure Determination of p4g Ni(100)-(2 × 2)C by LEED. *Surf. Sci.* **251**:493 (1991).

[6] J.H. Onuferko, D.P. Woodruff, and B.W. Holland. LEED Structure Analysis of the Ni{100}(2 × 2)C(p4g) Structure; a Case of Adsorbate-Induced Substrate Distortion. *Surf. Sci.* **87**:357 (1979).

[7] H.D. Shih, F. Jona, D.W. Jepsen, and P.M. Marcus. Metal-Surface Reconstruction Induced by Adsorbate: Fe(110)p(2 × 2)-S. *Phys. Rev. Lett.* **46**:731 (1981).

[8] N. Kruse and A. Gaussmann. Changes in the Morphology of Rh Field Emitter Tips due to the Reaction with Carbon Monoxide. *Surf. Sci.* **266**:51 (1992).

[9] J.E. Lennard-Jones. Processes of Adsorption and Diffusion on Solid Surfaces. *Trans. Faraday Soc.* **28**:333 (1932).

[10] T.H. Lin and G.A. Somorjai. Angular and Velocity Distributions of HD Molecules Produced by the H_2-D_2 Reaction on the Stepped Pt(557) Surface. *J. Chem. Phys.* **81**:704 (1984).

[11] J. Bardeen. The Image and van der Waals Forces at a Metallic Surfaces. *Phys. Rev.* **58**:727 (1940).

[12] H. Margenau and W.G. Pollard. The Forces between Neutral Molecules and Metallic Surfaces. *Phys. Rev.* **60**:128 (1941).

[13] D. Lando and L.J. Slutsky. Surface van der Waals Forces. *J. Chem. Phys.* **52**:1510 (1970).

[14] F. London. The General Theory of Molecular Forces. *Trans. Faraday Soc.* **33**:8 (1937).

[15] F. London. Zur Theorie und Systematik der Molekularkräfte. *Z. Phys.* **63:**245 (1930).

[16] P. Debye. Molekularkräfte und Ihre Elektrische Deutung. *Physikalische Zeitschrift*, **22:**302 (1921).

[17] P. Debye. Die van der Waalsschen Kohäsionskräfte. *Phys. Z.* **21:**178 (1920).

[18] W.H. Keesom. Die van der Waalsschen Kohäsionskräfte. Berichtigung. *Phys. Z.* **22:**643 (1921).

[19] W.H. Keesom. Die van der Waalsschen Kohäsionskräfte. *Phys. Z.* **22:**129 (1921).

[20] J.C. Slater and J.G. Kirkwood. Van der Waals Forces in Gases. *Phys. Rev.* **37:**682 (1931).

[21] F. London. Über einige Eigenschaften und Anwendungen der Molekularkräfte. *Z. Phys. Chem. Abt. B* **11:**222 (1930).

[22] A.D. Crowell. Surface Forces and the Solid-Gas Interface. In: E.A. Flood, editor, *The Solid-Gas Interface*, Volume 1. Marcel Dekker, New York, 1967.

[23] J.K. Nørskov. Chemisorption on Metal Surfaces. *Rep. Prog. Phys.* **53:**1253 (1990).

[24] G.A. Somorjai and B.E. Bent. The Structure of Adsorbed Monolayers. The Surface Chemical Bond. *Prog. Colloid Polym. Sci.* **70:**38 (1985).

[25] B.E. Bent. Bonding and Reactivity of Unsaturated Hydrocarbons on Transition Metal Surfaces: Spectroscopic and Kinetic Studies of Platinum and Rhodium Single Crystal Surfaces. Ph.D. thesis, University of California, Berkeley, 1986.

[26] C.M. Mate, G.A. Somorjai, H.W.K. Tom, X.D. Zhu, and Y.R. Shen. Vibrational and Electronic Spectroscopy of Pyridine and Benzene Adsorbed on the Rh(111) Crystal Face. *J. Chem. Phys.* **88:**441 (1988).

[27] E. Wimmer, C.L. Fu, and A.J. Freeman. Catalytic Promotion and Poisoning: All-Electron Local-Density-Functional Theory of CO on Ni(001) Surfaces Coadsorbed with K or S. *Phys. Rev. Lett.* **55:** 2618 (1985).

[28] D.J. Coulman, J. Winterlin, R.J. Behm, and G. Ertl. Novel Mechanism for the Formation of Chemisorption Phases: the (2 × 2)O—Cu(110) "Added Row" Reconstruction. *Phys. Rev. Lett.* **64:**1761 (1990).

[29] G.A. Somorjai. Directions of Theoretical and Experimental Investigations into the Mechanisms of Heterogeneous Catalysis. *Catal. Lett.* **9:**311 (1991).

[30] A. Wander, M.A. Van Hove, and G.A. Somorjai. Molecule-Induced Displacive Reconstruction in a Substrate Surface: Ethylidyne Adsorbed on Rh(111) Studied by Low-Energy-Electron Diffraction. *Phys. Rev. Lett.* **67:**626 (1991).

[31] S.M. Davis, F. Zaera, B.E. Gordon, and G.A. Somorjai. Radiotracer and Thermal Desorption Studies of Dehydrogenation and Atmospheric Hydrogenation of Organic Fragments Obtained from [^{14}C]Ethylene Chemisorbed over Pt(111) Surfaces. *J. Catal.* **92:**240 (1985).

[32] D. Godbey, F. Zaera, R. Yeates, and G.A. Somorjai. Hydrogenation of Chemisorbed Ethylene on Clean, Hydrogen, and Ethylidyne Covered Platinum (111) Crystal Surfaces. *Surf. Sci.* **167:**150 (1986).

[33] D.B. Kang and A.B. Anderson. Adsorption and Structural Rearrangements of Acetylene and Ethylene on Pt(111); Theoretical Study. *Surf. Sci.* **155:**639 (1985).

[34] B.E. Bent, C.M. Mate, J.E. Crowell, B.E. Koch, and G.A. Somorjai. Bonding and Thermal Decomposition of Propylene, Propadiene, and Methyl Acetylene on the Rh(111) Single-Crystal Surface. *J. Phys. Chem.* **91:**1493 (1987).

[35] D.E. Wilk, C.D. Stanners, Y.R. Shen, and G.A. Somorjai. The Structure and Thermal Decomposition of *Para-* and *Ortho*-Xylene on Pt(111). A HREELS, LEED, and TPD Study. *Surf. Sci.* (1993).

[36] J. Nakamura, J.M. Campbell, and C.T. Campbell. Kinetics and Mechanism of the

Water-Gas Shift Reaction Catalysed by the Clean and Cs-promoted Cu(110) Surface: A Comparison with Cu(111). *J. Chem. Soc. Faraday Trans.* **86:**2725 (1990).

[37] D.E. Gardin and G.A. Somorjai. The Vibrational Spectra (HREELS) and Thermal Decomposition (TPD) of Methylamine (CH_3NH_2) and Ethylamine ($C_2H_5NH_2$) on Ni(111). *J. Phys. Chem.* **96:**9424 (1992).

[38] G.A. Somorjai, C.M. Kim, and C. Knight. Building of Complex Catalysts on Single-Crystal Surfaces. In: D.J. Dwyer and F.M. Hoffmann, editors, *Surface Science of Catalysis: In Situ Probes and Reaction Kinetics. ACS Symposium Series*, Volume 482. American Chemical Society, Washington, D.C., 1992.

[39] J.E. Crowell. Chemical Modification of Surfaces: The Effect of Potassium on the Chemisorption of Molecules on Transition Metal Crystal Surfaces. Ph.D. thesis, University of California, Berkeley, 1984.

[40] C.M. Mate, C.T. Kao, and G.A. Somorjai. Carbon Monoxide Induced Ordering of Adsorbates on the Rh(111) Crystal Surface: Importance of Surface Dipole Moments. *Surf. Sci.* **206:**145 (1988).

[41] J.E. Crowell and G.A. Somorjai. The Effect of Potassium on the Chemisorption of Carbon Monoxide on the Rh(111) Crystal Face. *Appl. Surf. Sci.* **19:**73 (1984).

[42] J.E. Crowell, W.T. Tysoe, and G.A. Somorjai. Potassium Coadsorption Induced Dissociation of CO on the Rh(111) Crystal Face: An Isotope Mixing Study. *J. Phys. Chem.* **89:**1598 (1985).

[43] Y. Larher. Triple Point of the First Monomolecular Layer of Krypton Adsorbed on the Cleavage Face of Graphite. *J. Chem. Soc. Faraday Trans. I* **70:**320 (1974).

[44] A.W. Adamson. *Physical Chemistry of Surfaces*. John Wiley & Sons, New York, 1990.

[45] R. Miranda, S. Daiser, K. Wandelt, and G. Ertl. Thermodynamics of Xenon Adsorption on Pd(s) [8(100) × (110)]: From Steps to Multilayers. *Surf. Sci.* **131:**61 (1983).

[46] A. Atrei, U. Bardi, M. Maglietta, G. Rovida, M. Torrini, and E. Zanazzi. SEELFS Study of Ni(001)(2 × 2)C p4g Structure. *Surf. Sci.* **211/212:**93 (1989).

[47] J.C. Campuzano. The Adsorption of Carbon Monoxide by the Transition Metals. In: D.A. King and D.P. Woodruff, editors, *Chemisorption Systems, Part A. The Chemical Physics of Solid Surfaces and Heterogeneous Catalysis*, Volume 3. Elsevier, New York, 1990.

[48] A. Glachant, M. Jaubert, M. Bienfait, and G. Baoto. Monolayer Adsorption of Kr and Xe on Metal Surfaces: Structures and Uniaxial Phase Transitions on Cu(110). *Surf. Sci.* **115:**219 (1981).

[49] U. Bardi, A. Glachant, and M. Bienfait. Phase Transitions on Stepped and Disordered Surfaces: Xe Adsorbed on Cu and NaCl Single Crystal Surfaces. *Surf. Sci.* **97:**137 (1980).

[50] M.P. Kiskinova. *Poisoning and Promotion in Catalysis Based on Surface Science Concepts and Experiments. Studies in Surface Science and Catalysis*, Volume 70. Elsevier, Amsterdam, 1992.

[51] G.E. Rhead. On the Variation of Work Function with Coverage for Alkali-Metal Adsorption. *Surf. Sci.* **203:**L663 (1988).

[52] H.P. Bonzel. Alkali-Metal-Affected Adsorption of Molecules on Metal Surfaces. *Surf. Sci. Rep.* **8:**43 (1987).

[53] K. Christmann and J.E. Demuth. Interaction of Inert Gases with a Nickel (100) Surface. I. Adsorption of Xenon. *Surf. Sci.* **120:**291 (1982).

[54] Y.C. Chen, J.E. Cunningham, and C.P. Flynn. Dependence of Rare-Gas–Adsorbate Dipole Moment on Substrate Work Function. *Phys. Rev. B* **30:**7317 (1984).

[55] C.P. Flynn and Y.C. Chen. Work Function and Bonding Energy of Rare-Gas Atoms Adsorbed on Metals. *Phys. Rev. Lett.* **46**:447 (1981).

[56] H. Hong, C.J. Peters, A. Mak, R.J. Birgeneau, P.M. Horn, and H. Suematsu. Synchrotron X-Ray Study of the Structures and Phase Transitions of Monolayer Xenon on Single-Crystal Graphite. *Phys. Rev. B* **40**:4797 (1989).

[57] J. Suzanne, J.P. Coulomb, and M. Bienfait. Two-Dimensional Phase Transition in Xenon Submonolayer Films Adsorbed on (0001) Graphite. *Surf. Sci.* **47**:204 (1976).

[58] J. Suzanne, J.P. Coulomb, and M. Bienfait. Transition Bidimensionelle du Premier Ordre; Cas du Xénon Adsorbé sur la Face (0001) du Graphite. *Surf. Sci.* **44**:141 (1974).

[59] J. Suzanne, J.P. Coulomb, and M. Bienfait. Auger Electron Spectroscopy and LEED Studies of Adsorption Isotherms: Xenon on (0001) Graphite. *Surf. Sci.* **40**:414 (1973).

[60] A. Thomy, X. Duval, and J. Regnier. Two-Dimensional Phase Transitions as Displayed by Adsorption Isotherms on Graphite and Other Lamellar Solids. *Surf. Sci. Rep.* **1**:1 (1981).

[61] E.L. Muetterties, T.N. Rhodin, E. Band, C.F. Brucker, and W.R. Pretzer. Clusters and Surfaces. *Chem. Rev.* **79**:91 (1979).